Modeling Regional Air Quality and Climate: Improving Organic Aerosol and Aerosol Activation Processes in WRF/Chem version 3.7.1

Khairunnisa Yahya[1], Timothy Glotfelty[1], Kai Wang[1], Yang Zhang[1]*, and Athanasios Nenes[2,3,4,5]

[1]Department of Marine, Earth, and Atmospheric Sciences, North Carolina State University, Raleigh, North Carolina, U.S.A.
[2]School of Earth and Atmospheric Sciences, Georgia Institute of Technology, Atlanta, GA, U.S.A
[3]School of Chemical and Biomolecular Engineering, Georgia Institute of Technology, Atlanta, GA, U.S.A.
[4]Institute of Environmental Research & Sustainable Development, National Observatory of Athens, Greece
[5]Institute for Chemical Engineering Science, Foundation for Research and Technology-Hellas, Patra, Greece

Email: *yang_zhang@ncsu.edu

ABSTRACT

Air quality and climate influence each other through the uncertain processes of aerosol formation and cloud droplet activation. In this study, both processes are improved in the Weather, Research and Forecasting model with Chemistry (WRF/Chem) version 3.7.1. The existing Volatility Basis Set (VBS) treatments for organic aerosol (OA) formation in WRF/Chem is improved by considering the secondary OA (SOA) formation from semi-volatile primary organic aerosol (POA), a semi-empirical formulation for the enthalpy of vaporization of SOA, as well as functionalization and fragmentation reactions for multiple generations of products from the oxidation of VOCs. Two-month long simulations (May to June 2010) are conducted over continental U.S. and results are evaluated against surface and aircraft observations during the Nexus of Air Quality and Climate Change (CalNex) campaign. Among all the configurations considered, the best performance is found for the simulation with the 2005 Carbon Bond mechanism (CB05) and the VBS SOA module with semivolatile POA treatment, 25%

fragmentation, and the emissions of semi-volatile and intermediate volatile organic compounds being 3 times of the original POA emissions. Among the three gas-phase mechanisms (CB05, CB6, and SAPRC07) used, CB05 gives the best performance for surface ozone and $PM_{2.5}$ concentrations. Differences in SOA predictions are larger for the simulations with different VBS treatments (e.g., non-volatile POA versus semivolatile POA) as compared to the simulations with different gas-phase mechanisms. Compared to the simulation with CB05 and the default SOA module, the simulations with the VBS treatment improve cloud droplet number concentration (CDNC) predictions (NMBs from -40.8% to a range of -34.6% to -27.7%), with large differences between CB05/CB6 and SAPRC07 due to large differences in their OH and HO_2 predictions. An advanced aerosol activation parameterization based on the FN05 series reduces the large negative CDNC bias associated with the default ARG00 parameterization from -35.4% to a range of -0.8% to 7.1%. It, however, increases the errors due to overpredictions of CDNC, mainly over northeastern U.S. This work indicates a need to improve other aerosol-cloud-radiation processes in the model such as the spatial distribution of aerosol optical depth and cloud condensation nuclei in order to further improve CDNC predictions.

1. Introduction

The Intergovernmental Panel on Climate Change (IPCC) report on the AR5 scenario attributes the aerosol radiative forcing (RF) to be the dominant source of uncertainty contributing to the overall uncertainty in the net Industrial Era Radiative Forcing (RF) calculations (Myhre et al., 2013). Despite the inclusion of more aerosol processes in the current generation of atmospheric models, differences between atmospheric models and observations continue to persist. Aerosols affect the climate through the direct effect by absorbing or scattering radiation, or the indirect effect by acting as cloud condensation nuclei (CCN). According to Hallquist et al. (2009), the

formation of inorganic particulates such as sulfate, nitrate, and ammonium are well understood, however, there are large uncertainties in the formation of secondary organic aerosol (SOA). As a result, current models do not have a comprehensive treatment of OA, which usually result in an underprediction of OA concentrations (Hodzic et al., 2010; Jathar et al., 2011; Bergstrom et al., 2012), due to missing key precursors and processes in OA formation (Ahmadov et al., 2012). Some of the missing key precursors in most models include semi-volatile primary organic aerosol (POA), long-chain *n*-alkanes, polycyclic aromatic hydrocarbons (PAHs), and large olefins that have lower volatilities compared to traditional SOA precursors (Chan et al., 2009). The organic carbon (OC) component of the radiative forcing in the IPCC AR5 report also does not include SOA with the reason that the formation is dependent on a number of factors that are not currently sufficiently quantified (Myhre et al., 2013). However, SOA can form a significant percentage of total OA (up to 95% in rural areas) (Zhang et al., 2007). Another large source of uncertainty is the quantification of clouds as well as aerosol-cloud interactions due to incomplete or inaccurate representations of these processes in climate models (Boucher et al., 2013). A major process in cloud formation from aerosol is aerosol activation, which involves the condensational growth of aerosols in a cooling air parcel until maximum supersaturation, and some of the wet particles reach a critical radius where they are then able to grow spontaneously into cloud droplets (Ghan et al., 2011). Various approaches have been developed to reduce the uncertainties associated with OA and aerosol activation treatments in climate models. Those treatments are reviewed in the following section.

1.1. VBS Treatments and Sensitivity to Different Gas-Phase Chemical Mechanisms in Regional and Global Models

Unlike inorganic aerosols such as sulfate, the physical and chemical properties of OA dynamically evolve with age (Jimenez et al., 2009). The traditional approach to modeling SOA is

78 to assume that each VOC precursor forms several surrogate compounds (Odum et al., 1996).
79 However, the traditional method has several shortcomings, for example, two products are needed
80 for each VOC precursor causing this method to be computationally-expensive if many VOC
81 precursors are treated in the model (Murphy and Pandis, 2009). The assumption that the products
82 are unreactive also does not reflect the dynamic nature of the first generation products from the
83 oxidation of VOCs that can undergo successive oxidation steps to further produce lower volatility
84 products (Jimenez et al., 2009). The volatility basis set (VBS) is a framework developed by
85 Donahue et al. (2006), which is able to simulate gas-phase partitioning and multiple generations
86 of gas-phase oxidation of organic vapors. This approach addresses the shortcomings of the
87 traditional SOA modeling approach as it can cover the complete volatility range of OA compounds
88 (Murphy and Pandis, 2009).
89 Table 1 summarizes some of the VBS treatments from current regional and global models. The
90 VBS treatment has been implemented into a number of regional models such as the Weather,
91 Research and Forecasting model with Chemistry (WRF/Chem) (Shrivastava et al., 2011;
92 Ahmadov et al., 2012),the Particulate Matter Comprehensive Air Quality Model with extensions
93 (PMCAMx) (Lane et al., 2008; Donahue et al., 2009; Murphy et al., 2009), and CHIMERE (Hodzic
94 et al., 2010). It has also been implemented in global models such as GISS II' GCM (Farina et al.,
95 2010; Jathar et al., 2011) and the Community Earth System Model (CESM) (Shrivastava et al.,
96 2015). Different studies define the classifications of the organic species slightly differently.
97 Donahue et al. (2009) defined primary organic vapors with effective saturation concentrations (C*)
98 of 10^{-2} - 10^{-1}, 10^{0} - 10^{2}, and 10^{3} – 10^{6} µg m^{-3}at 298 K to be low volatility organic compounds
99 (LVOCs),semi-volatile organic compounds (SVOCs), and intermediate volatility organic
100 compounds (IVOCs), respectively. Shrivastava et al., (2011) and Jathar et al. (2011) defined

primary organic vapors with C* values of10^{-2} - 10^{3} and 10^{4} – 10^{6} μg m^{-3} to be SVOCs and IVOCs, respectively. All those studies defined VOCs to be gas-phase organic species with C* larger than 10^{6} μg m^{-3} at 298 K.

The traditional emission inventories used in the chemical transport models consist of VOCs but not SVOCs or IVOCs as both SVOCs and IVOCs are difficult to measure. This is most likely because SVOCs and IVOCs tend to evaporate at high temperatures from combustion sources (Donahue et al., 2009). As the traditional SOA approach usually underpredicts the SOA concentration, the addition of the SVOC and IVOC emissions on top of the existing VOC emissions in most emission inventories can improve model performance. To account for the missing key precursors in OA formation, SVOC and IVOC emissions are usually estimated as a factor of existing POA emissions in current emission inventories. For example, Shrivastava et al. (2011) estimated the sum of all SVOC and IVOC precursors to be 7.5 times the mass of traditional POA emissions inventory over Mexico City, but indicated that the scaling factor of 3 for SVOC emissions based on the POA emissions is poorly constrained. Shrivastava et al. (2008) and Jathar et al. (2011) assumed that SVOC emissions are represented by the traditional emission inventory while IVOC emissions are 1.5 times the traditional emission inventory. Pye and Seinfeld (2010) assumed that SVOC emissions are a subset of traditional POA emission inventories, and their POA emissions were scaled up by 27% on a global scale. IVOC emissions are assumed to be spatially-distributed similar to naphthalene and are predicted to be roughly a factor of half of global POA emissions. Tsimpidi et al. (2014) assumed that the IVOC emissions are 1.5 times the traditional POA emission inventory and are assigned to the 4^{th} volatility bin with C* = 10^{5} □g m^{-3}. For comparison, some studies such as Ahmadov et al. (2012) and Bergstrom et al. (2012) used the VBS approach for OA modeling but did not include additional SVOC emissions. There are also

differences in the volatility distribution used in literature. Shrivastava et al. (2008) and Jathar et al. (2011) found that moving half the mass of SVOC from all bins to the lowest bin from the traditional "diesel exhaust" volatility distribution of Robinson et al. (2007) produced the lowest errors in simulated OA on an annual average basis.

The number of bins used can also result in differences in simulated SOA concentrations. Shrivastava et al. (2011) showed that the 2-species VBS performed better than the 9-species VBS in modeling oxygenated organic aerosol (OOA) and gave the closest agreement to the OOA calculated by the Positive Matrix Factorization (PMF) method. This indicates that SOA may be less volatile as compared to the volatility distribution in the 9-species VBS which allows for evaporation of SOA with dilution (Shrivastava et al., 2011).

The amount of oxygen added for each oxidation step may contain uncertainties. This factor can influence the O:C ratio used for the model evaluation. O:C predictions from models need to be improved by including fragmentation reactions (which could lead to an increase in O:C ratios) and improving emission estimates (Shrivastava et al., 2011). Different rate constants can also result in different predictions of SOA concentrations. For example, Farina et al. (2010) showed that the use of k value of 1×10^{-12} cm^3 $molecule^{-1}$ s^{-1} compared to the default k value of10×10^{-12} cm^3 $molecule^{-1}$ s^{-1} resulted in a reduced aged SOA formation by 71%. Hodzic et al. (2010) also showed a case study based on Grieshop et al. (2009) in which each oxidation step reduced the volatility of the S/IVOC vapors by two orders of magnitude and each successive oxidation step produced a 40% increase in mass due to the addition of oxygen. This case is inconclusive in urban areas - a larger bias along with a higher correlation coefficient compared to the more common case where each oxidation step reduced the volatility by one order of magnitude with a 7.5% increase in mass.

146 However, the model performed worse (with larger bias and lower correlation coefficient) in
147 suburban areas.

148 The aging process improves model performance in general in the United States (U.S.) but
149 deteriorates the performance in several parts of Europe. Accounting for the aging process of OA
150 will increase the OA concentrations and improve model results in the U.S. where OA is usually
151 underpredicted, but increase the model bias for OA in several parts of Europe where OA
152 concentrations are overpredicted (Farina et al., 2010; Bergstrom et al., 2012).

153 Shrivastava et al. (2013) studied the effects of the fragmentation and functionalization in VBS.
154 Functionalization increases the mass of OA for each successive oxidation step, while
155 fragmentation reduces the mass for each oxidation step. One such a case includes simulating first-
156 order effects of the fragmentation and functionalization processes in VBS by assuming
157 functionalization of 100% of organic vapors for the first two generations of oxidation and both
158 fragmentation and functionalization for the third and higher generations of oxidation. The
159 fragmentation reduces the SOA concentrations drastically. For example, Shrivastava et al. (2013)
160 showed that peak SOA concentrations can be reduced by factors of 2 to 4 for a 1-hour example on
161 10 March 2006 at 21 UTC over Mexico City Plateau.

162 The VBS framework for OA modeling in the latest version of WRF/Chem, v3.7.1, is coupled
163 with several gas-phase mechanisms including the 2005 Carbon Bond Mechanism (CB05)
164 (Yarwood et al., 2005), the Model for Ozone and Related chemical Tracers version 4 (MOZART-
165 4) (Emmons et al., 2010), the Regional Atmospheric Chemistry Model (RACM) (Stockwell et al.,
166 1997), and the 1999 version of the Statewide Air Pollution Research Centre (SAPRC99)
167 mechanism (Carter, 2000). Different gas-phase mechanisms have different lumpings/groupings
168 for VOCs, which will affect OA formation. For example, VOCs are lumped according to their

carbon bonds (e.g., single or double bond) in CB05 (Yarwood et al., 2005) while VOCs in SAPRC99 (Carter, 2000) are lumped according to their OH reactivities. A number of studies examined the differences in predicting O_3 concentrations due to different gas-phase mechanisms (e.g., Luecken et al., 2008; Li et al., 2012; Shearer et al., 2012; Zhang et al., 2012), but fewer studies reported the impact of different gas-phase mechanisms on modeling SOA and $PM_{2.5}$ concentrations (Kim et al., 2011; Zhang et al., 2012). SAPRC99 has more detailed organic chemistry compared to CB05. SAPRC99 has been updated to SAPRC07 (and recently, to SAPRC11) based on newly available information regarding the reactions and influence of individual VOCs on O_3, as well as evaluations against chamber experiments (Carter, 2010). In addition, SAPRC07 has reformulated reactions of peroxy radicals so that the effects of changes in nitrogen oxides (NO_x) on organic product formation is more accurately represented. SAPRC07 has the most extensive set of VOC species and reactions, as compared to CB05 and the Carbon Bond version 6 (CB6). Shearer et al. (2012) reported that a condensed version of SAPRC07 predicted lower O_3 and OH concentrations in central California compared to SAPRC99 due to a decreased reaction rate coefficient in the reaction of OH and NO_2 to form HNO_3. Li et al. (2012) also showed that predicted O_3 concentrations from SAPRC07 were lower than those of SAPRC99 by up to 20% over Texas. The same study also reported that SAPRC07 gave lower OH concentrations due to differences in the reaction rate constants in the reactions of O^1D and H_2O between SAPRC07 and SAPRC99. Luecken et al. (2008) reported that SAPRC99 gave higher O_3 concentrations compared to CB05 on average; however, the differences vary with locations, VOC/NO_x ratios, and the concentrations of precursor pollutants. This is consistent with the results from Zhang et al. (2012), which predicted that SAPRC99 using WRF/Chem with the Model of Aerosol, Dynamics, Reaction, Ionization and Dissolution (WRF/Chem-MADRID) produced the

highest O_3 mixing ratios in July at the Southeastern Aerosol Research and Characterization (SEARCH) sites. The CB6 (Yarwood et al., 2010) is an updated version of CB05 with improved kinetic and photolysis data, additional explicit species for long-lived and abundant organic compounds including propane, acetone, benzene and acetylene, as well as revised isoprene and aromatics chemistry from CB05. Yarwood et al. (2010) showed that CB6 produces higher daily maximum 8-hr O_3 as compared to CB05 over Los Angeles for one episode day in August with the highest observed O_3 mixing ratios. CB6 was also shown to produce substantially higher OH concentrations (25% to 50% higher at mid-day over large areas) over eastern U.S. compared to CB05 over a few days in June, 2006. A summary of the main characteristics of CB05, CB6, and SAPRC07 gas-phase mechanisms are listed in Table 2.

1.2. Description of Aerosol Activation Parameterizations

Ghan et al. (2011) provided a comprehensive review on various aerosol activation treatments in current climate models. Two main types of parameterizations are commonly used: the Abdul-Razzak and Ghan (2000) (AR-G00) and the Fountoukis and Nenes (2005) (FN05) and associated updates described in Barahona et al. (2010) and Morales Betancourt and Nenes (2014). AR-G00 uses multiple lognormal or sectional distributions to approximate the aerosol size distribution. It uses the Kohler theory to relate the aerosol size distribution and composition to the number of aerosols activated as a function of maximum supersaturation (S_{max}). The complex function involving S_{max} is parameterized based on the standard deviation σ from a large number of numerical solutions using a cloud parcel model. The number and mass activated are particles with critical supersaturation less than S_{max}. It also accounts for particle growth before and after the particles are activated. However, the ARG treatment does not explicitly represent kinetic limitations which tend to affect smaller or larger particles (with diameters far from their critical

size). Very small particles tend to lose water when supersaturation declines as they never exceed the critical supersaturation for that particle size, and very large particles may not have achieved the critical size before S_{max} is reached (Ghan et al., 2011). Kinetic limitations refer to the (i) inertial mechanism – where particles with large dry diameters grow to be as large as activated particles but have not been activated themselves, these particles should be considered together with activated particles; (ii) evaporation mechanism – where particles with high critical supersaturation evaporate before reaching their critical diameters; and the (iii) deactivation mechanism – where initially activated particles that are deactivated to interstitial aerosols when the parcel supersaturation falls below the equilibrium supersaturation (Nenes et al., 2001). Neglecting kinetic limitations performs well for all conditions except in highly-polluted areas (Ghan et al., 2011). In urban and highly-polluted cases, many particles fail to be activated due to strong evaporation and deactivation processes (Nenes et al., 2001). Explicitly accounting for kinetic limitations reduces CDNC at low updraft velocity (Ghan et al., 2011).

The Fountoukis and Nenes (2005) (FN05) scheme improved the ARG00 scheme by solving S_{max} analytically (with the exception of kinetically-limited particles) using a so-called "population splitting" method. In addition, FN05 took into account the kinetic limitations, as well as the influence of gas kinetics on water vapor diffusivity (Ghan et al., 2011). The other improved treatments built on top of the FN05 scheme include the entrainment of ambient air, which could reduce the supersaturation of the updraft (Barahona and Nenes, 2007) (BN07) (therefore reducing CDNC); the adsorption of water vapor onto insoluble particles by Kumar et al. (2009) (KU09) based on a modified Frenkel-Halsey-Hill (FHH) adsorption theorem (which will increase CDNC); the growth of giant cloud condensation nuclei (CCN) (Barahona et al., 2010) (BA10) by introducing an additional condensation rate term to account for condensation of giant CCN (which

will reduce CDNC); as well as the modification of the original population splitting concept in FN05 and BA10 by Morales Betancourt and Nenes (2014) (MN14) by better accounting for the size of inertially limited CCN, and removing a discontinuity in the calculation of the surface area of cloud droplets.

The parameterization of Abdul Razzak and Ghan (2000) (ARG00) is used as the default aerosol activation module in WRF/Chem. It is not linked to the microphysics module or cumulus parameterization in WRF or WRF/Chem. However, for WRF/Chem, the cloud droplet number concentration (CDNC) generated in ARG00 is passed to the microphysics scheme, i.e., the Morrison two-moment microphysics scheme selected in this work.

1.3 Motivations and Objectives

The online-coupled meteorology and chemistry model, WRF/Chem, has recently been applied for air quality and climate modeling on a decadal scale (Yahya et al., 2016a, b). WRF/Chem can also simulate aerosol direct and indirect feedbacks, which are important considerations for climate modeling. However, as mentioned previously, the representations of OA and aerosol-cloud interactions in current regional and global climate models are subject to large uncertainties. In particular, while the VBS framework in WRF/Chem significantly improves SOA performance (Wang et al., 2015), it lacks the semi-volatile POA treatment, as well as fragmentation processes (Shrivastava et al., 2013). The first objective of this study is to reduce uncertainties associated with OA predictions by improving the existing VBS module in WRF/Chem and identifying the best gas-phase chemical mechanism to drive the VBS module for the most accurate OA predictions. The impact of the improved OA predictions on CDNC in WRF/Chem will be quantified. The second objective is to incorporate an improved aerosol

activation parameterization based on the FN05 series into WRF/Chem to study its impacts on CDNC predictions.

2. Model Configuration, Evaluation Protocol, and Observational Datasets

2.1.Model Setup and Inputs

The model used in this study is a modified version of WRF/Chem v3.7.1 as described by Wang et al. (2015). The 2005 Carbon Bond gas-phase mechanism (CB05) of Yarwood et al. (2005) with additional chlorine chemistry is coupled with the Modal for Aerosol Dynamics in Europe – Secondary Organic Aerosol Model (MADE/SORGAM) (Ackermann et al., 1998; Schell et al., 2001) and the Volatility Basis Set (MADE/VBS) (Ahmadov et al., 2012). The CB05-VBS option has also been coupled to existing model treatments including the aerosol direct effect, the aerosol semi-direct effect on photolysis rates of major gases, and the aerosol indirect effect on CDNC and resulting impacts on shortwave radiation. The physics options used in WRF/Chem include the rapid and accurate radiative transfer model for GCM (RRTMG) for both shortwave and longwave radiation, the Yonsei University (YSU) planetary boundary layer (PBL) scheme (Hong et al., 2006; Hong, 2010), the Morrison et al. (2009) double moment microphysics scheme, as well as the Multi-scale Kain-Fritsch (MSKF) cumulus parameterization scheme (Zheng et al., 2016). Aqueous-phase chemistry module (AQCHEM) for both resolved and convective clouds is based on a similar AQCHEM module in CMAQv4.7 of Sarwar et al. (2011). The anthropogenic emissions used are from the 2010 emissions based on the 2008 U.S. Environmental Protection Agency (U.S. EPA) National Emissions Inventory (NEI) from the Air Quality Model Evaluation International Initiative (AQMEII) project (Pouliot et al., 2015). Dust emissions are based on the Atmospheric and Environmental Research Inc. and Air Force Weather Agency (AER/AFWA) scheme (Jones and Creighton, 2011). Emissions from sea salt are generated based on the scheme of Gong et al. (1997).

Biogenic emissions are simulated online by the Model of Emissions of Gases and Aerosols from Nature v2.1 (MEGAN2.1) (Guenther et al., 2006).

The chemical initial and boundary conditions (ICONs/BCONs) come from the modified CESM/CAM version 5.3 with updates by Gantt et al. (2014), He and Zhang (2014), and Glotfelty et al. (2016). The meteorological ICONs/BCONs are from the National Center for Environmental Protection Final Reanalyses (NCEP FNL) dataset, which is available every 6 hours. The chemical fields are also allowed to run continuously while the meteorology is reinitialized every 5 days. The simulations are performed at a horizontal resolution of 36-km with 148 × 112 horizontal grid cells over the CONUS domain and parts of Canada and Mexico, and a vertical resolution of 34 layers from the surface to 100-hPa.

A number of sensitivity simulations are designed to identify the model configuration with results that are in the closest agreement to observations as well as the realistic model treatments of OA that are the closest to atmospheric processes. The baseline and sensitivity simulations are conducted from May to June 2010, during which the Nexus of Air Quality and Climate Change (CalNex) campaign was held in Bakersfield and Pasadena, California. The first 10 days from May 1st to May 10th are considered to be the spin-up period.

2.2. Model Evaluation Protocol and Available Measurements

Statistical measures including the Mean Bias (MB), Correlation Coefficient (Corr), Normalized Mean Bias (NMB) and Normalized Mean Error (NME) (Yu et al., 2006) are used to evaluate the simulations against observational data. Observational data are available for organic carbon (OC) and total carbon (TC) from the Speciated Trends Network (STN) and the Interagency Monitoring for Protected Visual Environments (IMPROVE). While both OC and TC from IMPROVE are used for model evaluation, only TC data from STN are used as STN uses the

311 thermo-optical transmittance protocol for OC that is different from the one used by IMPROVE
312 (Zhang et al., 2012). In addition, the measurements for STN OC are not blank corrected for carbon
313 on the background filter (Wang et al., 2012). The ratios OA/OC ratios vary across locations in the
314 continental U.S. (CONUS) depending on whether the OA is dominated by secondary formation
315 (Aitken et al., 2008) or it contains more aliphatic hydrocarbons (Turpin and Lim, 2001). In this
316 study, two ratios, 1.4 and 2.1, are used to convert simulated OA to OC based on a number of
317 studies in literature (Turpin and Lim, 2001; Aitken et al., 2008; Xu et al., 2015). As the simulations
318 are based on CONUS with varying OA properties (less or more oxidized OA), the use of two
319 OA/OC ratios can represent the different types of OA present for all locations in the U.S. Spatial
320 plots, time series plots at specific sites, as well as overlay plots are used to evaluate model
321 performance. The IMPROVE sites chosen for the time series plots include the visibility-protected
322 areas in Brigantine National Wildlife Refuge (NWR), NJ, Death Valley National Park (NP), CA,
323 Swanqwarter National Wildlife Refuge (NWR), NC, and the Tallgrass Prairie National Preserve,
324 KS. The Brigantine NWR is a tidal wetland and has a shallow bay, the Death Valley NP is a desert,
325 and the Swanqwarter NWR is a coastal brackish marsh. The time series plots are made at four STN
326 sites including two urban sites: in Washington, DC and Boise, ID, one industrial site in Tampa,
327 FL, and one rural/agricultural site in Liberty, KS. SOA, hydroxyl radical (OH) and hydroperoxy
328 radical (HO_2) data are also available for May to June 2010 as part of the California Research at the
329 Nexus of Air Quality and Climate Change (CalNex) campaign (Kleindienst et al., 2012;
330 Lewandowski et al., 2013) in Bakersfield, CA and Pasadena, CA, which are both urban locations.
331 The Bakersfield sampling site is located between the city center and areas of agricultural activity,
332 while the Pasadena site is located at the California Institute of Technology campus within the Los
333 Angeles metropolitan area to the southwest and mountains in the north (Baker et al., 2015).

POA/OA ratios are also used to evaluate the performance of the model. A number of studies have reported observed POA/OA ratios which range from 15% to 40% over CONUS. For example, over southeastern U.S., hydrocarbon-like OA (HOA) and cooking OA are found to contribute to 21 – 38% of total OA in urban sites (Xu et al., 2015). HOA and oxygenated OA (OOA) are found to account for 34% and 66% of measured OA from Pittsburgh in September 2002 (Zhang et al., 2005). HOA and cooking OA are assumed to be synonymous to POA, and OOA is assumed to be synonymous to SOA. Particulate matter sampled during August and September 2006 in Houston as part of the Texas Air Quality Study II Radical and Aerosol Measurement Project showed that approximately 32% of OA comes from HOA (Cleveland et al., 2012). Results from positive matrix factorization analysis from the Pasadena ground site during May and June 2010 showed that the primary components contribute 29% of the total OA mass (Hayes et al., 2013). Based on Zhang et al. (2007), the percentages of HOA mass at urban sites in Riverside, CA, from mid-July to mid-August 2005, in Houston, TX, from mid-August to mid-September 2000, and in New York City in July 2001 are 15%, 38%, and 30%, respectively. In addition, Zhang et al. (2011) compiled a large number of field campaigns across the globe where the average POA/OA ratios for urban, downwind and rural/remote areas are found to be 0.42, 0.18 and 0.10 respectively.

For the aerosol activation sensitivity and production simulations, additional variables that will be analyzed in this study include maximum 1-hour and 8-hour O_3 against the Clean Air Status and Trends Network (CASTNET) and Air Quality System (AQS), aerosol optical depth (AOD), CDNC and cloud condensation nuclei (CCN) against MODIS.

3. Model Development and Improvement

A number of modifications have been made to the standard version of WRF/Chem model v3.7.1. Those modifications and treatments are described below.

3.1. OA Treatments

The CB05-VBS treatment in the default WRF/Chem v3.7.1 assumes that POA is nonreactive and nonvolatile. In this study, POA is assumed to be semivolatile, and can undergo gas-particle partitioning, similar to anthropogenic SOA (ASOA) and biogenic SOA (BSOA) in VBS. While the volatility of ASOA and BSOA is represented by 4 bins with C* from 10^0 to 10^3 μg m^{-3}. The POA is distributed into 9 bins, with C* from 10^{-2} to 10^6 μg m^{-3}, following the set-up of Shrivastava et al. (2011). The POA is oxidized to form semi-volatile OA (SVOA), which can also undergo gas-particle partitioning. For the POA, bin-resolved enthalpies of vaporizations are used, ranging from 64 kJ mol^{-1} for the 9^{th} bin to 112 kJ mol^{-1} for the 1^{st} bin according to Shrivastava et al. (2011). The default enthalpy of vaporization (ΔH_{vap}) for SOA in WRF/Chem is 30 kJ mol^{-1} according to Lane et al. (2008). A more accurate alternative is to use the ΔH_{vap} values calculated from the semi-empirical correlation from Epstein et al. (2010):

$$\Delta H_{vap} = -11 \log_{10} C^*_{300} + 129 \quad (1)$$

The values of ΔH_{vap} Epstein et al. (2010) are used in a number of sensitivity simulations and final production simulation.

Shrivastava et al. (2013, 2015) also implemented several cases of fragmentation and functionalization (FF) processes into VBS. For this study, the FF set-up is similar to the method employed by Shrivastava et al. (2013), with the exception that fragmentation percentages of 10%, 25%, and 50% are used in sensitivity simulations. Shrivastava et al. (2013) used fragmentation percentages of 50% (intermediate fragmentation) and 85% (high fragmentation) in his simulations over Mexico City. For example, for the 10% FF case, 10% of the mass in the VBS species is

functionalized and moved to the next lower volatility bin, 80% is fragmented and moved to the highest volatility bin, and the remaining 10% is fragmented and becomes more volatile than the highest volatility bin (i.e., it is lost from the current volatility bins). For the 50% FF case, 50% is functionalized and moved to the next lower volatility bin, 40% is fragmented and moved to the highest volatility bin, and 10% is lost.

Zhao et al. (2014) measured IVOCs in Pasadena, CA during CalNex and found that the concentrations of primary IVOCs are similar to those of single-ring aromatics, and they produce about 30% of newly formed SOA in the afternoon. With the semivolatile POA and FF cases in this study, additional IVOC and SVOC emissions are added as three times of the traditional POA emissions from NEI, to account for missing IVOC and SVOC species in the traditional POA emission inventory. The fraction of IVOC/SVOC emissions assigned to each volatility bin is summarized in Table 3.

The mass fraction of organics in each volatility bin determined in laboratory studies also differs significantly according to the sources of organics. For example, May et al. (2013a, b, c) has different volatility distributions of mass fractions of organics for gasoline vehicle exhaust, diesel exhaust, and biomass burning. To take into account the different sources of organic compounds into a single volatility distribution for the purpose of this work, a new volatility distribution is calculated based on the mass fractions reported by Shrivastava et al. (2011), May et al. (2013a, c) and the percentages of VOC emissions from various sources from the 2008 NEI. According to the 2008 NEI report (Rao et al., 2013), total VOC emissions from stationary, mobile and fire (prescribed and wildfire) sources are ~7.6, ~5.6, and ~49.6 million tons, respectively. The corresponding percentages for VOC emissions are ~12%, ~9%, and ~79% for stationary, mobile, and fire sources, respectively. Based on the U.S. EPA (2013), the percentages of diesel emissions

404 from mobile sources are low compared to gasoline sources (~7% of total diesel and gasoline
405 sources); they are thus not included in this study.

406 An example calculation for the mass fraction of the lowest volatility bin for POA and
407 IVOC/SVOC emissions are as follows:

408 $$\text{Log } C_{-2}^{*} \text{ (at 298K)} = 0.04\times12\% + 0.14\times9\%+0.79\times79\% = 0.1754 \quad (2)$$

409 where C_{-2}^{*} refers to the lowest volatility bin with a value of 10^{-2} μg m^{-3}, 12%, 9%, and 79% refer
410 to the percentages for VOC emissions from stationary, mobile, and fire sources, respectively from
411 NEI, 0.04 refers to the original mass fraction for stationary emissions based on anthropogenic
412 emissions from Shrivastava et al. (2011) for the lowest volatility bin with a value of 10^{-2} μg m^{-3},
413 0.14 refers to the original mass fraction for gasoline emissions from May et al. (2013a) for the
414 lowest volatility bin with a value of 10^{-2} μg m^{-3}, 0.2 refers to the original mass fraction for biomass
415 burning emissions from May et al. (2013c) for the lowest volatility bin with a value of 10^{-2} μg m^{-3}
416, and 0.1754 refers to the newly-calculated mass fraction of POA and IVOC/SVOC emissions for
417 this study. The mass fractions used by Shrivastava et al. (2011), May et al. (2013a, c), and this
418 work can be found in Table 3.

419 **3.2. Gas-Phase Chemical Mechanisms**
420
421 Three gas-phase mechanisms are used: CB05, CB6, and SAPRC07. The gas-phase
422 mechanisms for CB6 and SAPRC07 are coupled to the MADE/VBS in WRF/Chem v3.7.1 in this
423 work following the coupling of CB05 with MADE/VBS by Wang et al. (2014). The emissions for
424 all cases are based on the CB05 chemical species from the 2010 emissions based on the 2008 NEI.
425 For SAPRC07, slight modifications had to be made to account for the different VOC species or
426 groups. The mapping of emission species from CB05 to SAPRC07 is based on the grouping of

427 species from emitdb.xls from Henderson et al. (2014) as well as from
428 http://www.cert.ucr.edu/~carter/emitdb/old-emitdb.htm. CB05 emissions are used for the CB6
429 case, with the exception of the VOCs including propane, benzene, ethyne, acetone, and ketone that
430 are mapped based on fractions of existing CB05 VOCs according to Yarwood et al. (2010).

431 In VBS, the SOA precursors for CB6 are similar to those for CB05. The SOA precursors for
432 CB05 (and therefore CB6) are mapped from the default SAPRC99 precursors by Wang et al.
433 (2015). The SAPRC07 SOA precursors follow the existing mapping of SAPRC99-MOSAIC/VBS
434 in WRF/Chem. The chemical equations and rate parameters from ENVIRON (2013) and Carter
435 (2010) for CB6 and SAPRC07 gas-phase mechanisms, respectively, were included in the
436 chem/KPP/mechanisms directory in WRF/Chem. The SAPRC07 gas-phase mechanism
437 implemented in WRF/Chem in this case is the uncondensed and expanded version C, which
438 includes reactions for peroxy radical operators (Carter, 2010). Species in both CB6-MADE/VBS
439 and SAPRC07-MADE/VBS undergo dry deposition, aqueous chemistry, photolysis, and wet
440 scavenging that are similar to CB05-MADE/VBS.

441 **3.3. Aerosol Activation**
442
443 The FN05 series aerosol activation parameterizations (with the exclusion of MN14) have been
444 incorporated into 3-D regional air quality models and global climate and Earth system models such
445 as the WRF-Community Atmosphere Model version 5 (WRF-CAM5) (Zhang et al., 2015), and in
446 the global-through-urban WRF/Chem (GU-WRF/Chem) (Zhang et al., 2012) and CESM (Gantt et
447 al., 2014). In this study, the FN series parameterizations are incorporated into WRF/Chem
448 following the methods of Gantt et al. (2014) and Zhang et al. (2015) as described in detail in Zhang
449 et al. (2015). However, in WRF/Chem, the aerosol activation module is only linked to the
450 microphysics module through the variable CDNC, which is read by the microphysics module. It

is not coupled to the cumulus parameterization scheme unlike in WRF-CAM5 and CESM. The FN05 series has been incorporated into module_mixactivate.F in the physics directory in WRF/Chem. As BN07 involves the entrainment effect for convective clouds and has very small impacts on non-convective CDNC (Zhang et al., 2015), it is not included in this study. In addition, unlike Gantt et al. (2014) and Zhang et al. (2015), the KU09 treatment is also not included in this study as the empirical constants A_{FHH} and B_{FHH} used in the formulation, which are compound-specific, have not been experimentally determined for black carbon, although those constants have been determined for dust and confirmed by Laaksonen et al. (2016). The additional MN14 treatment incorporated in this study involves a small modification to the original FN05 series parameterizations (without KU09), and helps to better account for the size of inertially limited CCN, and to remove a discontinuity in the calculation of the surface area of cloud droplets (Morales Betancourt and Nenes, 2014). The updated treatments are about 20% more computationally expensive to run as compared to ARG00 (Zhang et al., 2016), but capture the sensitivity of CDNC to all aspects of the aerosol with comparable accuracy to numerical parcel models, which was shown to be an underlying reason for biases from ARG (Morales Betancourt et al., 2014).

4. Results and Discussions

4.1.Sensitivity Simulations with VBS Treatments Coupled with CB05

As listed in Table 4, a number of sensitivity simulations are designed to identify the best model configuration for OA treatments with the closest agreement to observations over CONUS. Those sensitivity simulations consider (i) two SOA modules (MADE/SORGAM vs MADE/VBS), (ii) two types of VBS treatment for POA (nonvolatile POA versus semivolatile POA), (iii) two ΔH_{vap} treatments (default versus the semi-empirical ΔH_{vap} equation by Epstein et al. (2010)), (iv) three

different percentages of functionalization and fragmentation (FF) (10%, 25%, and 50%), (v) three sets of POA emissions (default versus 1.5 or 3 times the original NEI POA emissions), (vi) three different gas-phase mechanisms (CB05, CB6, and SAPRC07), and (vii) two different aerosol activation schemes (ARG00 versus combinations of different aerosol activation schemes of the FN05 series: FN05, FN05/BA10, and MN14) All simulations except for CB05-SORG-DH contain the VBS treatments for OA. CB05-SORG-DH and CB05-VBS-DH treat POA emissions as nonvolatile. In addition, the impact of two different cumulus parameterization schemes: Grell – Freitas (Grell and Freitas, 2014) and the Multi-scale Kain Fritsch (MSKF) (Zheng et al., 2016) scheme were also tested.

Table 5 summarizes the main statistics for all sensitivity simulations in terms of mean obs, mean sim, Corr, NMB, and NME for hourly OC and TC concentrations against IMPROVE and hourly TC concentrations against STN, respectively, over the whole CONUS domain. Figure 1 compares the domain mean hourly averaged observed OC or TC concentrations based on IMPROVE and STN with simulated concentrations calculated based on the ratios of OA/OC 1.4 and 2.1 for each sensitivity simulation. The domain mean hourly averaged obs OC concentration is 0.88 $\mu g\ m^{-3}$ for IMPROVE, and the domain mean hourly averaged obs TC concentration is 1.03 $\mu g\ m^{-3}$ for IMPROVE and 2.71 $\mu g\ m^{-3}$ for STN. As shown in Figure 1, the simulation CB05_SORG_DH with the default SOA module SORG largely underpredicts OC and TC with the largest NMBs and NMEs and the lowest Corr as compared to all other simulations with a SOA module based on the VBS method. The remaining VBS simulations significantly reduce the biases and errors in OC and TC from CB05_SORG_DH and also improve the correlation. Compared to CB05_SORG_DH, CB05_VBS_DH with nonvolatile POA seems to perform relatively well in terms of NMBs and Corr against IMPROVE OC, IMPROVE TC, and STN TC.

Adding the semivolatile POA treatment with 1.5 times the NEI POA emissions (CB05_POA_DH) reduces simulated OC and TC concentrations as compared to CB05_VBS_DH, due to the loss of mass from the semivolatile POA. As the POA mass is reduced, less surface area is available for SOA precursors to condense onto, resulting in decreased OA (thus decreased OC and TC) for CB05_POA_DH. Using the semi-empirical correlation of Epstein et al. (2010) for ΔH_{vap} increases the OC and TC concentrations (CB05_POA versus CB05_POA_DH). Compared to the default ΔH_{vap} of 30 kJ mol^{-1} used in CB05_POA_DH, the semi-empirical correlation of Epstein et al. (2010) gives much higher ΔH_{vap} values, resulting in more of the organic vapors in the particulate phase than in the gas phase. Compared to CB05-POA, the simulations with various FF treatments decrease the OA concentrations, as part of the OA mass is fragmented to higher volatility bins. The 10%FF case (CB05_10%FF) does not differ significantly from the no FF case (CB05_POA). However, increasing the percentage of FF (from 10% to 25%, then to 50%) decreases the OA concentrations. The FF treatments, however, even if they are more representative of actual SOA atmospheric formation processes, reduce the Corr slightly (compared to the cases CB05_POA and CB05-10%FF). By doubling the POA emissions (from 1.5 to 3.0 times the original POA NEI emissions) for the 25% FF case (CB05_FF25%_EM3), the predicted OC and TC concentrations are closer to the observations. When evaluated against IMPROVE OC, IMPROVE TC, and STN TC, among for simulations using CB05, the simulations CB05_VBS_DH, CB05_POA, CB05_FF10%, and CB05_FF25%_EM3 perform better than other cases. The differences in the OC and TC predictions from the simulations with different gas-phase mechanisms will be discussed later in Section 2.

Figure 2 shows the spatial distributions of simulated OC and TC concentrations overlaid with observed OC from IMPROVE and TC from STN for the case CB05_25%FF_EM3 for the two

OA/OC ratios. The model performs much better for IMPROVE OC with an OA/OC ratio of 2.1 as compared to 1.4, especially over eastern U.S. where the use of an OA/OC ratio of 1.4 results in large overpredictions. However over the central U.S. and parts of the western U.S., the use of an OA/OC ratio of 1.4 shows slightly better predictions of IMPROVE OC compared to the use of OA/OC ratio of 2.1 that gives underpredictions of OC. On the other hand, the model performs better for STN OC with an OA/OC ratio of 1.4 as compared to 2.1. The use of an OA/OC ratio of 1.4 gives better agreement with STN TC over eastern U.S. where the use of an OA/OC ratio of 2.1 results in large underpredictions of TC. Evaluation of OC and TC against IMPROVE and STN, respectively, therefore depends heavily on the OA/OC ratio, which is site-specific. Therefore in more rural sites (IMPROVE), the OA/OC ratio is more likely to be high (~2.1) with more oxygenated OA, while in more urban sites (STN), the OA/OC ratio is more likely to be lower (~1.4) due to fresher emissions and less oxidized species.

Figure 3 shows the POA/OA ratios for six sensitivity simulations. As mentioned earlier, the observed ratio of POA/total OA is approximately 15% to 40% during the summer period over various locations in the CONUS. As SOA concentrations from field campaigns are sparse at different locations and at different time periods, the POA/OA ratio is used to evaluate the model's capability to reproduce POA and SOA concentrations. The simulation CB05_SORG_DH with default SORGAM SOA module largely overpredicts the POA/OA ratio, due to significant underpredictions of SOA. The simulations CB05_VBS_DH, CB05_50%FF, and CB05_25%FF_EM3 with various VBS treatments all have POA/OA ratios that fall within the range of 0.15 to 0.4, with lower POA/OA ratios over more rural areas and higher POA/OA ratios over urban areas. CB05_VBS_DH, however, might give too high POA concentrations over the western portion of the domain as it does not consider POA to be semivolatile. Considering

545 semivolatile POA, however, without considering the fragmentation and functionalization
546 processes in the simulation CB05_POA results in too low POA/OA ratio (< 0.1 over most areas).
547 Similarly, the CB05_FF25% case also results in a large portion of CONUS with POA/OA ratios
548 of < 0.1, due to the loss of POA mass. CB05_FF50%, however, predicts reasonable POA/OA
549 ratios, even with fragmentation/functionalization due to balanced loss of both POA and SOA mass
550 through fragmentation to higher volatility bins. The simulation CB05_FF25%_EM3 also improves
551 from CB05_FF25% by increasing the POA mass contributing to higher POA/OA ratios.

552 Figure 4 shows the observed and simulated temporal variations of SOA concentrations at the
553 two CalNex sites: Bakersfield and Pasadena in CA from May to June 2010 for the simulations
554 CB05_SORM_DH, CB05_VBS_DH, CB05_25%FF_EM3, CB6_25%FF_EM3, and
555 SAPRC07_25%FF_EM3. There are large underpredictions of SOA by all runs on some days (e.g.
556 May 15 – 16, June 2 – 6, June 13 – 14) likely due to missing SOA precursor emissions. Table 6
557 shows the statistics of the simulations presented in Figure 4. The results using CB6 and SAPRC07
558 gas-phase mechanisms will be discussed in section 4.2. The observed SOA was derived based on
559 the tracer method of Kleindienst et al. (2012) which contains some uncertainties, and also likely
560 contributes to the poor correlation for most of the cases. For example, it assumes mass fraction of
561 the tracers in secondary organic carbon is the same in the field as that in the laboratory, and the
562 tracers are assumed to be inert and are unlikely to undergo oxidation in the atmosphere, which
563 might not be the case. In addition, the SOA data from the CalNex campaign only consider
564 contributions from a small number of precursors including biogenic precursors (i.e., isoprene, α-
565 pinene, and β-caryophyllene), and the anthropogenic precursors (i.e., toluene, polycyclic aromatic
566 hydrocarbons (PAHs) and methyl butenol (MBO)).

As shown in Figure 4 and Table 6, the simulation CB05_SORG_DH with the default SORGAM SOA module significantly underpredicts observed SOA concentrations at both sites. The model configuration of CB05_VBS_DH has been used in a number of WRF/Chem simulations published in literature (e.g., Yahya et al., 2015a; Campbell et al., 2015; Wang et al., 2015a, b). At Bakersfield, the simulation CB05_VBS_DH overpredicts the SOA concentrations for almost all the days. The simulation CB05_25%FF_EM3, however, underpredicts the SOA concentrations at Bakersfield, especially in June. The CB05_25%FF_EM3 case also shows low SOA concentrations throughout May and June, without much variability in SOA concentrations, likely due to underestimations of original POA emissions at Bakersfield. As the S/IVOC emissions for CB05_25%FF_EM3 are a factor of 3 of the original POA emissions from NEI, if the original POA emissions from NEI are underestimated, the S/IVOC emissions will be low, resulting in low SOA concentrations due to low concentrations of condensable material. At Pasadena, both CB05_VBS_DH and CB05_25%FF_EM3 overpredict the obs SOA from May 15th to May 30th, but are unable to capture the high SOA concentrations from 2nd to 6th June. The CB05_VBS_DH case seems to perform better than the CB05_25%FF_EM3 case when observed SOA concentrations are high. The results from this study are consistent with those from Baker et al. (2015), which showed that measured $PM_{2.5}$ OC at Bakersfield is largely underpredicted compared to Pasadena. Baker et al. (2015), however, attributed to the underpredictions of OC at Bakersfield and Pasadena mainly to primary OC predicted by the baseline model, as compared to the Aerosol Mass Spectrometer measurements, suggesting that OC is mostly secondary in nature in Pasadena. In addition, as mentioned earlier, the simulated SOA from WRF/Chem does not consider contributions from all the SOA precursors identified by their trace compounds (e.g., the biogenic precursor, b-caryophyllene, and the anthropogenic precursor MBO, are not included in

590 WRF/Chem), which can help to account for the discrepancies between the simulated and observed
591 SOA concentrations.

592 4.2. Sensitivity of OA predictions to different gas-phase mechanisms
593
594 Figure 1 shows that CB05_FF25%_EM3 produces the highest OC and TC concentrations at
595 the IMPROVE sites, followed by CB6_FF25%_EM3 and SAPRC07_FF25%_EM3, while
596 CB6_FF25%_EM3 produces the highest TC concentrations at the STN sites. However, the
597 differences in domain-mean simulated OC and TC between the simulations with the three different
598 gas-phase mechanisms are small, compared to the differences in simulated OC and TC due to
599 differences in VBS treatments (e.g., nonvolatile versus semivolatile POA). Figure 4 also shows
600 that there are not much differences between simulated SOA concentrations with different gas-
601 phase mechanisms at Bakersfield, but larger differences are found at Pasadena. . For example,
602 SAPRC07_25%FF_EM3 produces much higher SOA concentrations compared to
603 CB05_25%FF_EM3 and CB6_25%FF_EM3 at Pasadena on several days (e.g., June 6-8). Figure
604 5 shows the time series of hydroxyl radical (OH) mixing ratios as well as diurnal plots of OH and
605 hydroperoxyl radical (HO_2) at Pasadena from the CalNex field campaign. The time series of HO_2
606 is not shown due to irregularity of the observational data. The model is able to reproduce the
607 diurnal variation of OH radicals but significantly overpredicts the daytime and peak OH mixing
608 ratios, especially for CB05 and CB6. All gas-phase mechanisms underpredict OH mixing ratios at
609 night. Among all simulations, SAPRC07 produces the closest simulated OH mixing ratios
610 compared to CB05 and CB6 gives the largest overpredictions. Similarly, the HO_2 mixing ratios
611 are generally overpredicted by all gas-phase mechanisms with SAPRC07 performing the best. The
612 overpredictions in OH and HO_2 mixing ratios do not help explain the underpredictions of SOA for

several days at Pasadena where underpredictions of VOCs may be the main cause, which is consistent with the findings of Baker et al. (2015).

Figure 6 shows spatial distributions of average concentrations of oxidants including ozone (O_3), OH, HO_2, as well as the OA species including anthropogenic SOA (ASOA), biogenic SOA (BSOA), TSOA, and POA. SAPRC07-25%FF-EM3 produces the highest domain average O_3 mixing ratios but the lowest domain average $OH+HO_2$ mixing ratios while CB6-25%FF-EM3 produces the highest domain average and maximum $OH+HO_2$ mixing ratios but the lowest domain average O_3 mixing ratios. These findings are mostly consistent from literature. For example, maximum O_3 and OH mixing ratios over the Los Angeles area are higher for CB6 compared to CB05, which are consistent with the results from Yarwood et al. (2010). SAPRC07 also generally produces higher O_3 mixing ratios compared to CB05. However, average O_3 mixing ratios from CB6 are expected to be higher than CB05 (rather than lower as shown in Figure 6), according to the study from Nopmongcol et al. (2012) which showed higher O_3 mixing ratios over Europe for January and July using the Comprehensive Air Quality Model with Extensions (CAMx). CB6 is a relatively new gas-phase mechanism, there are very few studies that evaluated its performance over a longer period of time, e.g., for the whole summer, and over CONUS. In addition, there are other uncertainties in this study. For example, the emissions for CB05 are used for CB6, the additional explicit VOC species in CB6 such as benzene and acetylene are not considered, which can also contribute to O_3 formation. In addition, most locations in the U.S. in 2010 are considered to by NO_x-limited with localized VOC-limited regimes from May to September (Campbell et al., 2015), which means that O_3 formation is more likely to depend on NO_x rather than VOC concentrations.

Table 7 shows the statistics for maximum 1-hr and 8-hr O_3 mixing ratios evaluated against CASTNET and AQS. CASTNET sites are mainly rural sites, while AQS consists of urban, suburban, and rural sites. As expected, SAPRC07 consistently produces the highest maximum 1-hr and maximum 8-hr O_3 mixing ratios and overpredicts at AQS sites with an NMB of ~16%. However, SAPRC07 performs the best at CASTNET sites, as both CB05 and CB6 significantly underpredict maximum 1-hr and maximum 8-hr O_3 mixing ratios. At CASTNET sites, CB6 performs the poorest with the largest underpredictions for both maximum 1-hr and 8-hr O_3 mixing ratios. However, CB6 predicts higher maximum 1-hr and 8-hr O_3 mixing ratios at AQS sites, while CB05 predicts the lowest maximum 1-hr and 8-hr O_3 mixing ratios at AQS sites. It is likely that CB6 predicts higher O_3 mixing ratios at more VOC-limited sites in urban areas, while CB05 predicts higher O_3 mixing ratios at more NO_x-limited areas, due to the improvement in VOC speciation in CB6 compared to CB05. Overall, however, CB05 has the highest Corr and the lowest NMEs for CASTNET maximum 1-hr and AQS maximum 1-hr and 8-hr O_3 mixing ratios. For PM2.5 concentrations, CB6 produces the best performance against IMPROVE (highest Corr, lowest NMB and NME) while CB05 produces the best performance against STN (highest Corr and lowest NME). All 3 cases perform poorly for PM10 against AQS, with large underpredictions due to the non-consideration of the coarse mode inorganic species in MADE-VBS treatments.

Anthropogenic SOA (ASOA) concentrations are lower for CB6 and SAPRC07 compared to CB05. This is likely partially due to the emissions which are mapped from CB05 to CB6 and SAPRC07. The CB05 emissions are not likely to account for all anthropogenic VOC emissions in CB6 and SAPRC07, resulting in lower ASOA concentrations for CB6 and SAPRC07 compared to CB05. Biogenic SOA (BSOA) concentrations, however, are the largest for CB6, followed by SAPRC07 and CB05. BSOA concentrations are likely the highest for CB6 due to the highest

658 $OH+HO_2$ mixing ratios for CB6. The more extensive VOC representation and high O_3 mixing
659 ratios for SAPRC07 also likely contribute to the high BSOA concentrations for SAPRC07
660 compared to CB05. However, overall, the total SOA (TSOA) and POA concentrations for all three
661 gas-phase mechanisms do not vary much, resulting in similar OA concentrations.

662 Figures 7 and 8 show the time series of simulated versus observed OC from IMPROVE and
663 simulated versus observed TC from STN at several representative sites over CONUS for the
664 different gas-phase mechanisms. In general, at IMPROVE sites, CB05 gives the highest OC
665 concentrations compared to CB6 and SAPRC07 most of the time, resulting in overpredictions of
666 OC concentrations, while CB6 and SAPRC07 perform better against IMPROVE OC. The
667 overpredictions of CB05 are likely due to overpredictions in ASOA (as CB05 produces the highest
668 ASOA concentrations compared to CB6 and SAPRC07 as shown in Figure 6). As these sites are
669 located in rural locations, the dominant SOA is likely to be BSOA, or downwind ASOA from more
670 urban areas. With the exception of Death Valley NP, CA, the model performs relatively well in
671 predicting IMPROVE OC concentrations. Simulations with all three gas phase mechanisms
672 overpredict OC concentrations over several days in May in Brigantine NWR, Death Valley and
673 Swanqwarter, but is able to predict several of the peaks in June. All three gas-phase mechanisms,
674 however, largely underpredict OC concentrations over Death Valley from May 21st to June 30th.
675 As the Death Valley NP is a desert, the OC at Death Valley NP is most likely due to downwind
676 OC transported from upwind locations, for which the model is not able to capture due to
677 meteorological biases such as biases in wind fields. The differences between simulation results
678 from the gas-phase mechanisms are smaller for STN TC compared to IMPROVE OC, probably
679 due to similar elemental carbon (EC) concentrations for all gas-phase mechanisms, which can form
680 a significant percentage of TC. In general, all simulations with the three gas-phase mechanisms

also show similar trends (peaks and troughs) for simulated TC, likely due to influences from meteorological parameters such as wind and precipitation. Overall, all three simulations are also able to predict the magnitude and trends of STN TC concentrations relatively well. Similarly, CB05 tends to produce the highest TC concentrations, however, CB6 also does produce the highest TC concentrations for several days, for example, for some days in May in Washington, DC and Tampa, FL, as well as in June in Liberty, KS, likely due to influences of BSOA where CB6 produces the highest concentrations as shown in Figure 6.

4.3. Impact of Different VBS treatments on CDNC

Table 7 shows the statistics for model evaluation for simulated CDNC against MODIS-derived CDNC from Bennartz (2007) for May to June 2010. All simulations underpredict CDNC due likely to underpredictions in PM and CCN concentrations and uncertainties and/or assumptions in the derived CDNC based on MODIS retrievals of cloud properties by Bennartz (2007) (Zhang et al., 2015). For example, Bennartz (2007) derived the CDNC from cloud optical depths and cloud effective radius assuming adiabatically-stratified clouds. Among all simulations with CB05, CB05_SORG_DH produces the lowest CDNC due to underestimated OA concentrations. Increasing the OA concentrations helps to reduce the negative biases for CDNC. There are small differences, however, among simulated CDNC with different VBS treatments for CB05 in CDNC predictions, with similar Corr ~ 0.29, NMBs of ~-29% to -27% and NMEs of ~ 47%. Figure 9 shows the spatial differences in predictions in warm clouds between the several simulations and the simulation CB05_VBS_DH. CB05_SORGAM_DH gives the lower CDNC than CB05_VBS_DH, indicating that the VBS treatment in CB05_VBS_DH helps to increase CDNC significantly. While other simulations with semivolatile POA treatments further increase domain average CDNC comparing to CB05_VBS_DH, the differences between CDNC predictions from

those simulations and CB05_VBS_DH are quite similar. In general, CDNC with the semivolatile POA cases are higher over western U.S. but lower over eastern U.S. due to decreases in column OA concentrations for the semivolatile POA cases compared to CB05_VBS_DH over eastern U.S.

The large differences in CDNC predictions, however, are found between simulations with the different gas-phase mechanisms. SAPRC07_25%FF_EM3 has the largest negative bias (NMB of -52%) compared to all other simulations with CB05 and the simulation with CB6. Figure 10 compares the spatial plots for CDNC predictions for simulations with different gas-phase mechanisms, as well as the surface spatial plots for total OA and inorganic $PM_{2.5}$ concentrations. The simulation with SAPRC07 shows significantly lower CDNC over northeastern U.S. comparing to CDNC predictions from the other two simulations. While all three simulations show similar total OA concentrations, large differences are found for their total inorganic $PM_{2.5}$ concentrations, with SAPRC07 producing the lowest domain mean and maximum total inorganic $PM_{2.5}$ concentrations. Compared to CB05 and CB6, the lower inorganic $PM_{2.5}$ concentrations simulated with SAPRC07 are likely due to the low $OH+HO_2$ mixing ratios for SAPRC07 as shown in Figure 6, resulting in a lower PM number concentration and lower cloud condensation nuclei (CCN), thus lower CDNC.

4.4.Sensitivity Simulations for Aerosol Activation Parameterizations

Among all OA sensitivity simulations, the simulation CB05-25%FF-EM3 gives an overall best performance in terms of OC, TC, O_3, $PM_{2.5}$, and CDNC evaluation, it is thus selected to test various aerosol activation parameterizations. As listed in Table 4, four sensitivity simulations are designed to test the FN05 series aerosol activation parameterizations with improved treatments comparing to the default ARG00 aerosol activation parameterization. These sensitivity simulations include the default ARG00, the FN05, the combination of FN05 and BA10, and the MN14. These

729 simulations use the MSKF scheme instead of the Morrison microphysics schemes in the previous
730 SOA runs as the MSKF scheme has a better correlation with MODIS CDNC as compared to the
731 Morrison microphysics scheme. Table 8 summarizes the model evaluation results against MODIS-
732 derived CDNC from Bennartz (2007). The simulation ARG00 underpredicts CDNC with an NMB
733 of -35%. The FN05 series helps to reduce the underpredictions of CDNC significantly, because
734 they in general give higher activation fractions compared to the ARG00 parameterization under
735 most atmospheric conditions (Ghan et al., 2011). The addition of BA10 to the FN05 takes into
736 account the effects of condensation on giant CCN, which reduces the CDNC predictions and leads
737 to a negligible underprediction of CDNC (with an NMB of -0.8%) compared to a slight
738 overprediction by the FN05 with an NMB of 7.1%. MN14, which revises the original population
739 splitting method in FN05 and BA10, slightly increases the CDNC to an NMB of 4.2% comparing
740 to the FN05/BA10 simulation. The trends in the predictions of FN05, BA10, and MN14 are
741 consistent with the reported bias of ~+8%, -10% and -3%, respectively, by Morales Betancourt
742 and Nenes (2014) against the CDNC concentrations simulated from the cloud parcel model.
743 However, the Corr and NME are worse with the FN05 series and MN14. The NMEs are almost
744 doubled for the FN05 series and MN14, compared to that from the default ARG00. Figure 11
745 compares the spatial distributions of the simulated CDNC in warm clouds from ARG00, FN05
746 series, and MN14 and the MODIS-derived CDNC from Bennartz (2007). As shown in Figure 11,
747 the lower Corr and higher NMEs for the FN05 series as compared to ARG00 shown in Table 9, as
748 compared to ARG00, are due to the large overpredictions over northeastern U.S. but
749 underpredictions over other parts of the domain. The simulated CDNC from the default ARG00
750 case is similar to that from Bennartz (2007) over eastern U.S., the underpredictions are mainly
751 over western U.S. and over the ocean because of the known bias when large CCN are not present

(Morales Betancourt et al., 2014). The simulations with the FN05 series increase CDNC where CCN is high, i.e., over the northeastern U.S., resulting in overpredictions in CDNC over northeastern U.S., and does not help to improve CDNC predictions over other parts of the U.S. as well as over the ocean.

Figure 12 compares the simulated CCN and AOD from the CB05_25%FF_EM3 + MN14 case with those derived from the MODIS. The model largely underpredicts CCN, especially over the western part of the domain, which explains the large underprediction of CDNC also over the western part of the domain. Condensation of the available water vapor occurs over CCN which are concentrated over northeastern U.S., resulting in overpredictions of CDNC over northeastern U.S. The lack of CCN over the ocean and the western part of the domain is related to the underpredictions of AOD over the same areas. This indicates biases in number (and probably mass) concentrations of column PM concentrations, especially over the ocean and western U.S. $PM_{2.5}$ and PM_{10} observational data are available over the surface and are both underpredicted, however, there are no observational data for column concentrations of $PM_{2.5}$ and PM_{10} for evaluation. Improving the spatial distribution and magnitude of emissions for PM species and precursors for the model layers at the surface and above the surface can help improve AOD and CCN predictions, therefore CDNC predictions.

5. Summary and Conclusions

Current regional air quality models including WRF/Chem have large uncertainties in modeling OA and aerosol-cloud feedback mechanisms such as the aerosol activation process. Comparing to the traditional OA method, the VBS treatment helps to improve OA predictions by reducing the underpredictions of OA. By including a semivolatile POA treatment, using a semi-empirical formation of Epstein et al. (2010) for ΔH_{vap}, including 25% fragmentation and functionalization

776 as well as including additional S/IVOC emissions, the VBS treatment in WRF/Chem simulates the
777 atmospheric OA formation processes more realistically and can perform relatively well in
778 predictions of OC and TC against IMPROVE and STN. POA/OA ratios for the
779 CB05_25%FF_EM3 and CB05_FF50% treatments are within the range of POA/OA ratios of
780 ~0.15 to 0.40 from literature. Compared to the simulation with default SORGAM SOA module,
781 the simulations with various new VBS treatments also give better agreement with observed SOA
782 at Bakersfield and Pasadena during the CalNex field campaign from May to June 2010. However,
783 biases exist in those simulations with the VBS treatments due to several possible reasons, including
784 underestimated POA emissions, underpredicted VOC concentrations, as well as differences in the
785 SOA precursors used in the model and those contributing to the observed SOA concentrations.
786 The simulations with different gas-phase mechanisms (i.e., CB05, CB6, and SAPRC07) produce
787 in general different ASOA and BSOA concentrations. SAPRC07 produces the highest O_3 mixing
788 ratios, while CB6 produces the lowest OH + HO_2 mixing ratios. CB6 also performs the best when
789 evaluated against IMPROVE PM2.5 while CB05 performs the best when evaluated against STN
790 PM2.5 concentrations. All 3 cases perform poorly against AQS PM10 evaluation. Due to the
791 significant differences between O_3, OH, and HO_2 mixing ratios for the three gas-phase
792 mechanisms, inorganic PM concentrations vary widely, especially between the carbon bond
793 mechanisms (CB05 and CB6) and SAPRC07, resulting in significantly different predictions of
794 CDNC. The CDNC predictions do not vary much among simulations with CB05 and different
795 VBS treatments, for example, for simulations with nonvolatile versus semivolatile POA, and with
796 and without fragmentation and functionalization treatments. The simulation with SAPRC07
797 produces the lowest CDNC compared to those with CB05 and CB6, due to the lowest inorganic
798 PM number and mass concentrations resulted from the lowest OH and HO_2 mixing ratios among

all simulations. CB05 gives the best performances when evaluated against CASTNET and AQS ozone mixing ratios, STN $PM_{2.5}$ concentrations and against MODIS CDNC.

With the default ARG00 treatment in the model, in general, all simulations with VBS treatments underpredict the MODIS-derived CDNC by Bennartz (2007). By including the FN05 series (i.e., FN05, FN05/BA10, and MN14), the underpredictions for CDNC are greatly reduced. However, the correlation coefficient and errors are worse with the FN05 series, with large overpredictions over the northeastern U.S., where CCN is high. The model performs poorly for AOD and CCN, likely due to inaccuracies in spatial distribution and magnitudes of PM and PM precursor emissions in the model layers at the surface and above the surface. The CDNC predictions can be improved by improving AOD and CCN undepredictions over western U.S. and over the ocean.

Code and Data Availability

The WRF/Chem v3.7.1 code used in this paper will be available upon request. The inputs including the meteorological files, meteorological initial and boundary conditions, chemical initial and boundary conditions, model setup and configuration, and the namelist setup and instructions on how to run the simulations for a 1-day test case, as well as a sample output for a 1-day test, can be provided upon request.

Acknowledgments

This study is funded by the National Science Foundation EaSM program (AGS-1049200) at NCSU. The emissions are taken from the 2008 NEI-derived emissions for 2010 provided by the U.S. EPA, Environment Canada, and Mexican Secretariat of the Environment and Natural Resources (Secretaría de Medio Ambiente y Recursos Naturales-SEMARNAT) and National Institute of Ecology (Instituto Nacional de Ecología-INE) as part of the Air Quality Model

Evaluation International Initiative (AQMEII). The authors acknowledge use of the WRF-Chem preprocessor tool mozbc provided by the Atmospheric Chemistry Observations and Modeling Lab (ACOM) of NCAR and the script to generate initial and boundary conditions for WRF based on CESM results provided by Ruby Leung, PNNL. This work also used the Stampede Extreme Science and Engineering Discovery Environment (XSEDE) high-performance computing support which is supported by the National Science Foundation grant number ACI-1053575. The authors also acknowledge high-performance computing support from Yellowstone (ark:/85065/d7wd3xhc) provided by NCAR's Computational and Information Systems Laboratory, sponsored by the National Science Foundation and Information Systems Laboratory.

References

Abdul-Razzak, H., and Ghan, S.J.: A parameterization of aerosol activation 2. Multiple aerosol types, J. Geophys. Res., 105, D5, 6837 – 6844, 2000.

Ackermann, I.J., Hass, H., Memmesheimer, M., Ebel, A., Binkowski, F.S., and Shankar, U,: Modal aerosol dynamics model for Europe: Development and first applications, Atmospheric environment, 32, No.17, 2981-2999, 1998.

Ahmadov, R., McKeen, S.A., Robinson, A.L., Bareini, R., Middlebrook, A.M., De Gouw, J.A., Meagher, J., Hsie, E.-Y., Edgerton, E., Shaw, S., and Trainer, M.: A volatility basis set model for summertime secondary organic aerosols over the eastern United States in 2006, J. Geophys. Res., 117, doi:10.1029/2011JD016831, 2012.

Aitken, A.C., DeCarlo, P.F., Kroll, Worsnop, D.R., Huffman, J.A., Docherty, K.S., Ulbrich, I.M., Mohr, C., Kimmel, J.R., Sueper, D., Sun, Y., Zhang, Q., Trimborn, A., Northway, M., Ziemann, P.J., Canagaratna, M.R., Onasch, T.B., Alfarra, M.R., Prevot, A.S.H., Dommen, J., Duplissy, J., Metzger, A., Baltensperger, U., and Jimenez, J.L.: O/C and OM/OC Ratios of primary, secondary, and ambient organic aerosols with high-resolution time-of-flight aerosol mass spectrometry, Environ. Sci. Technol., 42(12), 4478 – 4485, doi:10.1021/es703009q, 2008.

Atkinson, R., Baulch, D.L., Cox, R.A., Crowley, J.N., Hampson, R.F., Hynes, R.G., Jenkin, M.E., Kerr, J.A., Rossi, M.J., and Troe, J.: "Evaluated kinetic and photochemical data for atmospheric chemistry - IUPAC subcommittee on gas kinetic data evaluation for atmospheric chemistry." July 2005 web version available from http://www.iupackinetic.ch.cam.ac.uk/index.html, 2005.

Atkinson, R.A., Baulch, D.L., Cox, R.A., Crowley, J.N., Hampson, R.F., Hynes, R.G., Jenkin, M.E., Kerr, J.A., Rossi, M.J., and Troe, J.: "Evaluated kinetic and photochemical data for atmospheric chemistry - IUPAC subcommittee on gas kinetic data evaluation for atmospheric chemistry." January 3, 2010 web version available at http://www.iupac-kinetic.ch.cam.ac.uk/index.html, 2010.

Baker, K.R., Carlton, A.G., Kleindienst, T.E., Offenberg, J.H., Beaver, M.R., Gentner, D.R., Goldstein, A.H., Hayes, P.L., Jimenez, J.L., Gilman, J.B., de Gouw, J.A., Woody, M.C., Pye, H.O.T., Kelly, J.T., Lewandowski, M., Jaoui, M., Stevens, P.S., Brune, W.H., Lin, Y-H., Rubitschun, C.L., and Surratt, J.D.: Gas and aerosol carbon in California: comparison of measurements and model predictions in Pasadena and Bakersfield, Atmos. Chem. Phys., 15, 5243 – 5258, doi:10.5194/acp-15-5243-2015, 2015.

Barahona, D., and Nenes, A.: Parameterization of cloud droplet formation in large-scale models: Including effects of entrainment, J. Geophys. Res., 112, D16206, doi:10.1029/2007JF008473, 2007.

Barahona, D., West, R.E.L., Stier, P., Romakkaniemi, S., Kokkola, H., and Nenes, A.: Comprehensively accounting for the effect of giant CCN in cloud activation parameterizations, Atmos. Chem. Phys., 10, 2467 – 2473, 2010.

Bennartz, R.: Global assessment of marine boundary layer cloud droplet number concentration from satellite, J. Geophys. Res. Atmos., 112, D02201, doi:10.1029/2006JD007547, 2007.

Bergstrom, R., Denier van der Gon, H.A.C., Prevot, A.S.H., Yttri, K.E., and Simpson, D.: Modelling of organic aerosols over Europe (2002 – 2007) using a volatility basis set (VBS) framework: application of different assumptions regarding the formation of secondary organic aerosol, Atmos. Chem. Phys., 12, 8499 – 8527, doi:10.5194/acp-12-8499-2012, 2012.

Boucher, O., Randall, D., Artaxo, P., Bretherton, C., Feingold, G., Forster, P., Kerminen, V.-M., Kondo, Y., Liao, H., Lohmann, U., Rasch, P., Satheesh, S.K., Sherwood, S., Stevens, B., and Zhang, X.Y.: Clouds and Aerosols. In: Climate Change 2013: The Physical Science Basis. Contribution of Working Group I to the Fifth Assessment Report of the Intergovernmental Panel on Climate Change [Stocker, T.F., D. Qin, G.-K. Plattner, M. Tignor, S.K. Allen, J. Boschung, A. Nauels, Y. Xia, V. Bex and P.M. Midgley (eds.)]. Cambridge University Press, Cambridge, United Kingdom and New York, NY, USA, 2013.

Campbell, P., Zhang, Y., Yahya, K., Wang, K., Hogrefe, C., Pouliot, G., Knote, C., Hodzic, A., San Jose, R., Perez, J.L., Jimenez Guerrero, P., Baro, R., and Makar, P.: A multi-model assessment for the 2006 and 2010 simulations under the Air Quality Model Evaluation International Initiative (AQMEII) phase 2 over North America: Part I. Indicators of the sensitivity of O_3 and $PM_{2.5}$ formation regimes, Atmos. Environ., 115, 569 – 586, 2015.

Carter, W.P.L.: Implementation of the SAPRC-99 chemical mechanism into the models-3 framework, Report to the US EPA (http://www.cert.ucr.edu/~carter/pubs/s99mod3.pdf), 2000. Last accessed, February 19, 2016.

892 Carter, W.P.L.: Development of the SAPRC07 chemical mechanism, Atmos. Environ., 44, 5324
893 – 5335, doi:10.1016/j.atmosenv.2010.01.026, 2010.

894 Chan, A.W.H., Kautzman, K.E., Chhabra, P.S., Surratt, J.D., Chan, M.N., Crounse, J.D., Kurten,
895 A., Wennberg, P.O., Flagan, R.C., and Seinfeld, J.H.: Secondary organic aerosol formation
896 from photooxidation of naphthalene and alkylnapthalenes: implications for oxidation of
897 intermediate volatility organic compounds (IVOCs), Atmos. Chem. Phys., 9, 3049-3060, 2009.

898 Cleveland, M.J., Ziemba, L.D., Griffin, R.J., Dibb, J.E., Anderson, C.H., Lefer, B., and
899 Rappengluck, B.: Characterization of urban aerosol using aerosol mass spectrometry and
900 proton nuclear magnetic resonance spectroscopy, Atmos. Environ., 54, 511 – 518,
901 doi:10.1016/j.atmosenv.2012.02.074, 2012.

902 Donahue, N.M., Robinson, A.L., Stanier, C.O., and Pandis, S.N.: Coupled partitioning, dilution
903 and chemical aging of semivolatile organics, Environ. Sci. Tech., 40, 2635 – 2643, 2006.

904 Donahue, M.N., Robinson, A.L., and Pandis, S.N.: Atmospheric organic particulate matter: From
905 smoke to secondary organic aerosol, Atmos. Environ. 43, 94-106, 2009.

906 Emmons, L.K., Walters, S., Hess, P.G., Lamarque, J.-F., Pfister, G.G., Fillmore, D., Granier, C.,
907 Guenter, A., Kinnison, D., Laepple, T., Orlando, J., Tie, X., Tyndall, G., Wiedinmyer, C.,
908 Baughcum, S.L., and Kloster, S.: Description and evaluation of the Model for Ozone and
909 Related chemical Tracers, version 4 (MOZART-4), Geosci. Model Dev., 3, 43 – 67, 2010.

910 ENVIRON: User's guide to the comprehensive air quality model with extensions, version 6, 2013.
911 Available at www.camx.com/files/camxusersguide_v6-10.pdf

912 Epstein, S.A., Riipinen, I., and Donahue, N.M.: A semiempirical correlation between enthalpy of
913 vaporization and saturation concentration for organic aerosol, Environ. Sci. Technol., 44, 743
914 – 748, 2010.

915 Farina, S.C., Adams, P.J., and Pandis, S.N.: Modeling global secondary organic aerosol formation
916 and processing with the volatility basis set: Implications for anthropogenic secondary organic
917 aerosol, J. Geophys. Res., 115, D09202, doi:10.1029/2009JD013046, 2010.

918 Fountoukis, C., and Nenes, A.: Continued development of a cloud droplet formation
919 parameterization for global climate models, J. Geophys. Res., 110, D11212,
920 doi:10.1029/2004JD00591, 2005.

921 Gantt, B., He, J., Zhang, X., Zhang, Y., and Nenes, A.: Incorporation of advanced aerosol
922 activation treatments into CESM/CAM5: model evaluation and impacts on aerosol indirect
923 effects, Atmos. Chem. Phys., 14, 7485 – 7497, doi:10.5194/acp-14-7485-2014, 2014.

924 Ghan, S.J., Abdul-Razzak, H., Nenes, A., Ming, Y., Liu, X., Ovchinnikov, M., Shipway, B.,
925 Meskhidze, N., Xu, J., and Shi, X.: Droplet nucleation: Physically-based parameterizations and
926 comparative evaluation, J. Adv. Model. Earth Syst., 3, M10001, doi:10.1029/2011ms000074,
927 2011.

928 Glotfelty, T., He, J. and Zhang, Y.: Updated organic aerosol treatments in CESM/CAM5:
929 development and initial application, in preparation, 2016.

930 Gong, S., Barrie, L.A. and Blanchet, J.P.: Modeling sea salt aerosols in the atmosphere: 1. Model
931 development, J. Geophys. Res., 102, 3805-3818, doi:10.1029/96JD02953, 1997.

932 Grell, G.A. and Freitas, S.R.: A scale and aerosol aware stochastic convective parameterization
933 for weather and air quality modeling, Atmos. Chem. Phys., 14, 5233-5250, doi:10.5914/acp-
934 14-5233-2014, 2014.

935 Grieshop, A.P., Logue, P., Donahue, J.M., Robinson, A.L., Laboratory investigation of
936 photochemical oxidation of organic aerosol from wood fires 1: measurement and simulation
937 of organic aerosol evolution, Atmos. Chem. Phys., 9, 1263-1277, 2009.

938 Guenther, A., Kart, T., Harley, P., Wiedinmyer, C., Palmer, P.I. and Geron, C.: Estimates of global
939 terrestrial isoprene emissions using MEGAN (Model of Emissions of Gases and Aerosols from
940 Nature), Atmos. Chem. Phys., 6, 3181-3210, 2006.

941 Hallquist, M., Wenger, J.C., Baltensperger, U., Rudich, Y., Simpson, D., Claeys, M., Dommen, J.,
942 Donahue, N.M., George, C., Goldstein, A.H., Hamilton, J.F., Herrman, H., Hoffman, T.,
943 Iinuma, Y., Jang, M., Jenkin, M.E., Jimenez, J.L., Kiendler-Scharr, A., Maenhaut, W.,
944 McFiggans, G., Mentel, T.F., Monod, A., Prevot, A.S.H., Seinfeld, J.H., Surratt, J.D.,
945 Szmigielski, R., and Wildt, J.: The formation, properties and impact of secondary organic
946 aerosol: current and emerging issues, Atmos. Chem. Phys., 9, 5155 – 5236, 2009.

947 Hayes, P.L., Ortega, A.M., Cubison, M.J., Froyd, K.D., Zhao, Y., Cliff, S.S., Hu, W.W., Toohey,
948 D.W., Flynn, J.H., Lefer, B.L., Grossberg, N., Alvarez, S., Rappengluck, B., Taylor, J.W.,
949 Allan, J.D., Holloway, J.S., Gilman, J.B., Kuster, W.C., de Gouw, J.A., Massoli, P., Zhang,
950 X., Liu, J., Weber, R.J., Corrigan, A.L., Russell, L.M., Isaacman, G., Worton, D.R., Kreisberg,
951 N.M., Goldstein, A.H., Thalman, R., Waxman, E.M., Volkamer, R., Lin, Y.H., Surratt, J.D.,
952 Kleindienst, T.E., Offenberg, J.H., Dusanter, S., Griffith, S., Stevens, P.S., Brioude, J.,
953 Angevine, W.M., and Jimenez, J.L.: Organic aerosol composition and sources in Pasadena,
954 California during the 2010 CalNex campaign, J. Geophys. Res. Atmos., 118, 9233–9257,
955 doi:10.1002/jgrd.50530, 2013.

956 He, J., and Zhang, Y.: Improvement and further development in CESM/CAM5: gas-phase
957 chemistry and inorganic aerosol treatments, Atmos. Chem. Phys., 14, 9171 – 9200,
958 doi:10.5194/acp-14-9171-2014, 2014.

959 Henderson, B.H., Akhtar, F., Pye, H.O.T., Napelenok, S.L., and Hutzell, W.T.: A database and
960 tool for boundary conditions for regional air quality modeling: description and evaluation,
961 Geosci. Model Dev., 7, 339 – 360, doi:10.5194/gmd-7-339-2014, 2014.

962 Hodzic, A., Jimenez, J.L., Madronich, S., Canagaratna, M.R., DeCarlo, P.F., Kleinman, L., and
963 Fast, J.: Modeling organic aerosols in a megacity: potential contribution of semi-volatile and

964 intermediate volatility primary organic compounds to secondary organic aerosol formation,
965 Atmos. Chem. Phys., 10, 5491-5514, 2010.

966 Hong, S.-Y., Noh, Y. and Dudhia, J.: A new vertical diffusion package with an explicit treatment
967 of entrainment processes, Mon. Wea. Rev., 134, 2318-2341, 2006.

968 Hong, S.-Y.: A new stable boundary-layer mixing scheme and its impact on the simulated East
969 Asian summer monsoon, Q.J.R. Meteorol. Soc., 136, 1481 – 1496, doi:0.1002/qj.665, 2010.

970 IUPAC: "Evaluated Kinetic and Photochemical Data". IUPAC Subcommittee on Gas Kinetic Data
971 Evaluation for Atmospheric Chemistry. Web Version. Available at
972 http://www.iupackinetic.ch.cam.ac.uk. Latest data sheets dated June, 2006.

973 Jathar, S.H., Farina, S.C., Robinson, A.L., and Adams, P.J.: The influence of semi-volatile and
974 reactive primary emissions on the abundance and properties of global organic aerosol, Atmos.
975 Chem. Phys., 11, 7727 – 7746, doi:10.5194/acp-11-7727-2011, 2011.

976 Jimenez, J.L., Canagaratna, M.R., Donahue, N.M., Prevot, A.S.H., Zhang, Q., Kroll, J.H.,
977 DeCarlo, P.F., Allan, J.D., Coe, H., Ng, N.L., Aiken, A.C., Docherty, K.S., Ulbrich, I.M.,
978 Grieshop, A.P., Robinson, A.L., Duplissy, J., Smith, J.D., Wilson, K.R., Lanz, V.A., Hueglin,
979 C., Sun, Y.L., Tian, J., Laaksonen, A., Raatikainen, T., Rautiainen, J., Vaattovaara, P., Ehn,
980 M., Kulmala, M., Tomlinson, J.M., Collins, D.R., Cubison, M.J., Dunlea, E.J., Huffman, J.A.,
981 Onasch, T.B., Alfarra, M.R., Williams, P.I., Bower, K., Kondo, Y., Schneider, J., Drewnick,
982 F., Borrman, S., Weimer, S., Demerjian, K., Salcedo, D., Cottrell, L., Griffin, R., Takami, A.,
983 Miyoshi, T., Hatakeyama, S., Shimono, A., Sun, J.Y., Zhang, Y.M., Dzepina, K., Kimmel,
984 J.R., Sueper, D., Jayne, J.T., Herndon, S.C., Trimborn, A.M., Williams, L.R., Wood, E.C.,
985 Middlebrook, A.M., Kolb, C.E., Baltensperger, U., and Worsnop, D.R.: Evolution of Organic
986 Aerosols in the Atmosphere, Science, 326 (5959), 1525 – 1529, doi:10.1126/science.1180353,
987 2009.

988 Jones, S. and Creighton, G.: AFWA dust emission scheme for WRF/Chem-GOCART, 2011 WRF
989 workshop, June 20-24, Boulder, CO, USA, 2011.

990 Kim, Y., Sartelet, K., and Seigneur, C.: Formation of secondary aerosols over Europe: comparison
991 of two gas-phase mechanisms, Atmos. Chem. Phys., 11, 583 – 598, doi:10.5194/acp-11-583-
992 2011, 2011.

993 Kleindienst, T.E., Jaoui, M., Lewandowski, M., Offenberg, J.H., and Docherty, K.S.: The
994 formation of SOA and chemical tracer compounds from the photooxidation of naphthalene and
995 its methyl analogs in the presence and absence of nitrogen oxides, Atmos. Chem. Phys., 8711
996 – 8726, doi:10.5194/acp-12-8711-2012, 2012.

997 Laaksonen, A., Malila, J., Nenes, A., Hung, H.Mop., Chen, J.P.: Surface fractal dimension, water
998 adsorption efficiency, and cloud nucleation activity of insoluble aerosol, *Nat.Sci.Rep.*, **6**,
999 25504, doi:10.1038/srep25504, 2016.

1000 Lane, T.E., Donahue, N.M., and Pandis, S.N.: Simulating secondary organic aerosol formation
1001 using the volatility basis-set approach in a chemical transport model, 42, 7439 – 7451, 2008.

1002 Lewandowski, M., Piletic, I.R., Kleindienst, T.E., Offenberg, J.H., Beaver, M.R., Jaoui, M.,
1003 Docherty, K.S., and Edney, E.O.: Secondary organic aerosol characterisation at field sites
1004 across the United States during the spring-summer period, Intern. J. Environ. Anal. Chem.,
1005 doi:10.1080/030674, 2013.

1006 Li, J., Zhang, H., and Ying, Q.: Comparison of the SAPRC07 and SAPRC99 photochemical
1007 mechanisms during a high ozone episode in Texas: Differences in concentrations, OH budget
1008 and relative response factors, Atmos. Environ., 25 – 35, doi:10.1016/j.atmosenv.2012.02.034,
1009 2012.

1010 Luecken, D.J., Phillips, S., Sarwar, G., and Jang, C.: Effects of using the CB05 versus SAPRC99
1011 versus CB4 chemical mechanism on model predictions: Ozone and gas-phase photochemical
1012 precursor concentrations, Atmos. Environ., 42, 5805 – 5820, 2008.

1013 May, A.A., Presto, A.A., Hennigan, C.J., Nguyen, N.T., Gordon, T.D., and Robinson, A.L.: Gas-
1014 particle partitioning of primary organic aerosol emissions: (1) Gasoline vehicle exhaust,
1015 Atmos. Environ., 77, 128 – 139, 2013a.

1016 May, A.A., Presto, A.A., Hennigan, C.J., Nguyen, N.T., Gordon, T.D., and Robinson, A.L.: Gas-
1017 particle partitioning of primary organic aerosol emissions: (2) Diesel vehicles, Environ. Sci.
1018 Tech., 47, 8288 – 8296, 2013b.

1019 May, A.A., Levin, E.J.T., Hennigan, C.J., Riipinen, I., Lee, T., Collett Jr., J.R., Jimenez, J.L.,
1020 Kreidenweis, S.M., and Robinson, A.L.: Gas-particle partitioning of primary organic aerosol
1021 emissions, 3. Biomass burning, J. Geophys. Res., 118, 11327 – 11338, doi:10.1002/jgrd.50828,
1022 2013c.

1023 Morales Betancourt, R., and Nenes, A.: Droplet activation parameterization: the population-
1024 splitting concept revisited, Geosci. Model Dev., 7, 2345 – 2357, doi:10.5194/gmd-7-2345-
1025 2014, 2014.

1026 Morrison, H., Thompson, G. and Tatarskii, V.: Impact of cloud microphysics on the development
1027 of trailing stratiform precipitation in a simulated squall line: Comparison of One- and Two-
1028 Moment Schemes, Mon. Wea. Rev., 137, 991-1007, 2009.

1029 Murphy, B.N., and Pandis, S.N.: Simulating the formation of semivolatile primary and secondary
1030 organic aerosol in a regional chemical transport model, Environ. Sci. Technol., 2009, 43, 4722
1031 – 4728, 2009.

1032 Myhre, G., Shindell, D., Breon, F.-M., Collins, W., Fuglestvedt, F., Huang, J., Koch, D.,
1033 Lamarque, J.-F., Lee, D., Mendoza, B., Nakajima, T., Robock, A., Stephens, G., Takemura,
1034 T., and Zhan, H.: Anthropogenic and Natural Radiative Forcing in: Climate Change 2013: The
1035 Physical Science Basis. Contribution of Working Group I to the Fifth Assessment Report of

the Intergovernmental Panel on Climate Change [Stocker, T.F., D. Qin, G.-K. Plattner, M. Tignor, S.K. Allen, J. Boschung, A. Nauels, Y. Xia, V. Bex and P.M. Midgley (eds.)]. Cambridge University Press, Cambridge, United Kingdom and New York, NY, USA, 2013.

Nenes, A. Ghan, S., Abdul-Razzak, H., Chuang, P.Y., and Seinfeld, J.: Kinetic limitations on cloud droplet formation and impact on cloud albedo, Tellus (2001), 53B, 133 – 149, 2001.

Nopmongcol, U., Koo, B., Tai, E., Jung, J., Piyachaturawat, P., Emery, C., Yarwood, G., Pirovano, G., Mitsakou, C., and Kallos, G.: Modeling Europe with CAMx for the Air Quality Model Evaluation International Initiative (AQMEII), Atmos. Environ., 53, 177 – 185, 2001.

Odum, J.R., Hoffman, T., Bowman, F., Collins, D., Flagan, R.C., and Seinfeld, J.H.: Gas/Particle Partitioning and Secondary Organic Aerosol Yields, Environ. Sci. Tech., 30(8), 2580 – 2585, doi:10.1021/es950943+, 1996.

Pouliot, G., van der Gon, H.D., Kuenen, J., Makar, P., Zhang, J., and Moran, M.: Analysis of the emission inventories and model-ready emission datasets for Europe and North America for phase 2 of the AQMEII project, Atmos. Environ., 115, 345 – 360, 2015.

Pye, H. and Seinfeld, J.H.: A global perspective on aerosol from low-volatility organic compounds, Atmos. Chem. Phys., 10, 4377 – 4401, doi:10.5194/acp-10-4377-2010, 2010.

Rao, V., Tooly, L., and Drukenbrod, J.: 2008 National Emissions Inventory: Review, Analysis and Highlights, EPA-454/R-13-005, accessed online at http://www.epa.gov/ttn/chief/net/2008report.pdf, 2013, last access October 9th, 2015.

Sander, S.P., Friedl, R.R., Golden, D.M., Kurylo, M.J., Huie, R.E., Orkin, V.L., Moortgat, G.K., Ravishankara, A.R., Kolb, C.E., Molina, M.J., and Finlayson-Pitts, B.J.: Chemical Kinetics and Photochemical Data for use in Atmospheric Studies, Evaluation Number 14. NASA Jet Propulsion Laboratory. February. Available from http://jpldataeval.jpl.nasa.gov/download.html, 2013.

Sander, S.P., Friedl, R.R., Golden, D.M., Kurylo, M.J., Moortgat, G.K., Wine, P.H., Ravishankara, A.R., Kolb, C.E., Molina, M.J., Finlayson-Pitts, B.J., Huie, R.E., and Orkin, V.L.: "Chemical Kinetics and Photochemical Data for use in Atmospheric Studies, Evaluation Number 15. NASA Jet Propulsion Laboratory." July. Available from http://jpldataeval.jpl.nasa.gov/download.html, 2006.

Sarwar, G., Fahey, K., Napelenok, S., Roselle, S. and Mathur, R.: Examining the impact of CMAQ model updates on aerosol sulfate predictions, the 10th Annual CMAS Models-3 User's Conference, October, Chapel Hill, NC, 2011.

Schell B., Ackermann, I.J., Hass, H., Binkowski, F.S., and Ebel, A.: Modeling the formation of secondary organic aerosol within a comprehensive air quality model system, J. Geophys. Res. 106, 28275-28293, 2001.

1071 Shearer, S.M., Harley, R.A., Jin, L., and Brown, N.J.: Comparison of SAPRC99 and SAPRC07
1072 mechanisms in photochemical modeling for central California, Atmos. Environ., 46, 205 –
1073 216, doi:10.1016/j.atmosenv.2011.09.079, 2012.

1074 Shrivastava, M.K., Lane, T.E., Donahue, N.M., Pandis, S.N., and Robinson, A.L.: Effects of gas
1075 particle partitioning and aging of primary emissions on urban and regional organic aerosol
1076 concentrations, J. Geophys. Res., 113, D18301, doi:10.1029/2007JD009735, 2008.

1077 Shrivastava, M., Fast, J., Easter, R., Gustafson Jr., W.I., Zaveri, R.A., Jimenez, J.L., Saide, P. and
1078 Hodzic, A.: Modeling organic aerosols in a megacity: comparison of simple and complex
1079 representations of the volatility basis set approach, Atmos. Chem. Phys., 11, 6639 – 6662,
1080 doi:10.5194/acp-11-6639-2011, 2011.

1081 Shrivastava, M., Zelenyuk, A., Imre, D., Easter, R., Beranek, J., Zaveri, R.A., and Fast, J.:
1082 Implications of low volatility SOA and gas-phase fragmentation reactions on SOA loadings
1083 and their spatial and temporal evolution in the atmosphere, J. Geophys. Res. Atmos., 118, 3328
1084 – 3342, doi:10.1002/jgrd.50160, 2013.

1085 Shrivastava, M., Easter, R.C., Liu, X., Zelenyuk, A., Singh, B., Zhang, K., Ma, P.-L., Chand, D.,
1086 Ghan, S., Jimenez, J.l., Zhang, Q., Fast, J., Rasch, P.J., and Titta, P.: Global transformation
1087 and fate of SOA: Implications of low-volatility SOA and gas-phase fragmentation reactions,
1088 J. Geophys. Res. Atmos., 120, 4169 – 4195, doi:10.1002/2014JD022563, 2015.

1089 Stockwell, W., Kirchner, F., Kuhn, M., and Seefeld, S.: A new mechanism for regional
1090 atmospheric chemistry modeling, J. Geophys. Res., 102, D22, 25847 – 25879, 1997.

1091 Tsimpidi, A.P., Karydis, V.A., Zavala, M., Lei, W., Molina, L., Ulbrich, I.M., Jimenez, J.L., and
1092 Pandis, S.N.: Evaluation of the volatility basis-set approach for the simulation of organic
1093 aerosol formation in the Mexico City metropolitan area. Atmospheric Chemistry and Physics
1094 10, 525-546, 2010.

1095 Turpin, B.J., and Lim, H.-J.: Species Contributions to PM2.5 Mass concentrations: Revisiting
1096 Common Assumptions for Estimating Organic Mass, Aero. Sci. Technol., 35, 1, 602 – 610,
1097 doi:10.1080/02786820119445, 2001.

1098 US EPA: 2008 National Emissions Inventory, version 3 Technical Support Document, September
1099 2013, Draft, accessed online at
1100 http://www3.epa.gov/ttn/chief/net/2008neiv3/2008_neiv3_tsd_draft.pdf, 2013, last accessed
1101 October 10th, 2015.

1102 Wang, K., and Zhang, Y.: Application, evaluation, and process analysis of the US EPA's 2002
1103 Multiple-Pollutant Air Quality Modeling Platform, Atmos. And Clim. Sci., 2, 254 – 289, 2012.

1104 Wang, K., Zhang, Y., Yahya, K., Wu, S.-Y., and Grell, G.: Implementation and initial application
1105 of new chemistry-aerosol options in WRF/Chem for simulating secondary organic aerosols

and aerosol indirect effects, Atmos. Environ., 115, 716 – 723, doi:10.1016/j.atmosenv.2015.12.007, 2015.

Xu, L., Guo, H., Boyd, C.M., Klein, M., Bougiatioti, A., Cerully, K.M., Hite, J.R., Isaacman-VanWertz, G., Kreisberg, N.M., Knote, C., Olson, K., Koss, A., Goldstein, A.H., Hering, S.V., de Gouw, J., Baumann, K., Lee, S.-H., Nenes, A., Weber, R.J., and Ng, N.L.: Effects of anthropogenic emissions on aerosol formation from isoprene and monoterpenes in the southeastern United States, Proc. Natl. Acad. Sci., 112, 1, 37 – 42, doi:10.1073/pnas.1417609112, 2015.

Yahya, K., Wang, K., Campbell, P., Glotfelty, T., He, J., and Zhang, Y.: Decadal evaluation of regional climate, air quality and their interactions over the continental US using WRF/Chem version 3.6.1, Geosci. Model Dev., 9, 671 – 695, doi:10.5194/gmd-9-671-2016, 2016a.

Yahya, K., Campbell, P., Chen, Y., Glotfelty, T., Pirhalla, M., and Zhang, Y.: Downscaling CESM using WRF/Chem: Decadal Application for Regional Air Quality and Climate Modeling over the U.S. under the Representative Concentration Pathways Scenarios, in preparation, 2016b.

Yarwood, G., Rao, S., Yocke, M., and Whitten, G.Z.: Final Report – Updates to the Carbon Bond Chemical Mechanism: CB05, Rep. RT-04-00675, 246 pp., Yocke and Co., Novato, CA, 2005.

Yarwood, G., Whitten, G.Z., Jung, J., Heo, G., and Allen, D.T.: Final Report – Development, Evaluation and Testing of Version 6 of the Carbon Bond Chemical Mechanism (CB6): Work Order No. 582-7-84005-FY10-26, ENVIRON, Novato, CA, 2010.

Yu, S., Eder, B., Dennis, R., Chu, S.-H., and Schwartz, S.: New unbiased symmetric metrics for evaluation of air quality models, Atmos. Sci. Lett., 7, 26 – 34, 2006.

Zhang, Q., Worsnop, D.R., Canagaratna, M.R., and Jimenez, J.L.: Hydrocarbon-like and oxygenated organic aerosols in Pittsburgh: insight into sources and processes of organic aerosols, Atmos. Chem. Phys., 5, 3289 – 3311, doi:10.5194/acp-5-3289-2005, 2005.

Zhang, Q., Jimenez, J.L., Canagaratna, M.R., Allan, J.D., Coe, H., Ulbrich, I., Alfarra, M.R., Takami, A., Middlebrook, A.M., Sun, Y.L., Dzepina, K., Dunlea, E., Docherty, K., DeCarlo, P.F., Salcedo, D., Onasch, T., Jayne, J.T., Miyoshi, T., Shimono, A., Hatakeyama, S., Takegawa, N., Kondo, Y., Schneider, J., Drewnick, F., Borrmann, S., Weimer, S., Demerjian, K., Williams, P., Bower, K., Bahreini, R., Cottrell, L., Griffin, R.J., Rautiainen, J., Sun, J.Y., Zhang, Y.M., and Worsnop, D.R.: Ubiquity and dominance of oxygenated species in organic aerosols in anthropogenically-influenced Northern Hemisphere midlatitudes, Geophys. Res. Lett., 34, L13801, doi:10.1029/2007GL029979, 2007.

Zhang, Q., Jimenez, J.L., Canagaratna, M.R., Ulbrich, I.M., Ng, N.L., Worsnop, D.R., and Sun, Y.: Understanding atmospheric organic aerosols via factor analysis of aerosol mass spectrometry: a review, Anal. Bioanal. Chem., 401(10), 3045 – 3067, doi:10.1007/s00216-011-5355-y, 2011.

Zhang, Y., Chen, Y.-C., Sarwar, G., and Schere, K.: Impact of gas-phase mechanisms on WRF/Chem predictions: Mechanism implementation and comparative evaluation, J. Geophys. Res., 117, D01301, doi:10.1029/2011JD015775, 2012.

Zhang, Y., Zhang, X., Wang, K., He, J., Leung, L.R., Fan, J., and Nenes, A.: Incorporating an advanced aerosol activation parameterization into WRF-CAM5: Model evaluation and parameterization intercomparison, J. Geophys. Res. Atmos., 120, doi:10.1002/2014JD023051, 2015.

Zhao, Y., Hennigan, C.J., May, A.A., Tkacik, D.S., de Gouw, J.A., Gilman, J.B., Kuster, W.C., Borbon, A., and Robinson, A.L.: Intermediate-volatility organic compounds: A large source of secondary organic aerosol, Environ. Sci. Technol., 48, 13743 – 13750, doi:10.1021/es5035188, 2014.

Zheng, Y., Alapaty, K.A., Herwehe, J.A., Del Genio, A.D., and Niyogi, D.: Improving high-resolution weather forecasts using the Weather Research and Forecasting (WRF) Model with an updated Kain-Fritsch scheme, Mon. Wea. Rev., 144, 833 – 860, doi:10.1175/mwr-d-15-0005.1, 2016.

Tables

Table 1. Summary of several literature studies of VBS treatments in various regional and global models.

Source	Ahmadov et al., 2012	Shrivastava et al., 2011	Farina et al., 2010	Jathar et al., 2011	Hodzic et al., 2010
Model	WRF-Chem	WRF-Chem	GISS II' GCM	GISS II' GCM	CHIMERE
Domain	CONUS	Mexico City	Global	Global	Mexico City
Spatial Resolution	20 km and 60 km	Nested 3 km within 12 km	$4^o \times 5^o$	$4^o \times 5^o$	5 km × 5 km and 35 km × 35 km
Emissions of SVOCs, IVOCs, and VOCs	Only VOCs; no emissions of SVOCs and IVOCs	SVOC emissions 3 times POA emissions for both anthropogenic and biomass burning emissions. IVOC emissions 1.5 times POA emissions	POA is treated as nonvolatile and nonreactive, but acts as absorbing phase for SOA condensation, forming 1 OA phase	SVOC emissions are represented by the traditional emission inventory. IVOC emissions are 1.5 times traditional emissions	SVOC emissions 3 times POA emissions. IVOC emissions 1.5 times POA emissions
No. of VBS bins	4	2 and 9	4	9	9
Aging	Yes and No Simulations with aging: each oxidation step produces 7.5% additional mass	Yes and No Simulations with aging: each oxidation step produces 15% additional mass	Yes	Yes and No. Each oxidation step does not produce any additional mass	Yes. 2 cases below: (i)Each oxidation step produces 7.5% additional mass (ii)Each oxidation step reduces the volatility by 2 orders of magnitude and 40% of additional mass produced
Observational data	SEARCH, STN, IMPROVE	MILAGRO 2006 field campaign	IMPROVE, EMEP	IMPROVE, FAME, MILAGRO, SOAR	MILAGRO 2006 field campaign
Variables evaluated	OC and EC	OA, HOA, OOA O:C ratio	OM:OC of 1.8	OA (surface), HOA, OOA	HOA, OOA, BBOA, O:C ratio
Summary of results with VBS framework with/without aging compared to the traditional SOA approach	-Improved diurnal variability -Results without the aging process underestimate OC throughout the day	-HOA and OOA: Lower negative bias with addition of S/IVOC emissions -OOA: 2 bin VBS better results than 9 bin VBS -Underprediction of O:C ratio in both cases	-IMPROVE: improved with aging -EMEP: aging further biases already high OA predictions	-Adding IVOC emissions improves performance, however underprediction remains in winter months	-HOA overpredicted during nighttime -Case(i):Modeled O:C 3 times lower than observed -Case(ii):Better agreement for O:C but SOA generally overestimated

Note: HOA: Hydrocarbon-like OA – Reduced specie of OA, generally understood as a surrogate for urban combustion-related POA; OOA: Oxygenated OA – Characterized by its high oxygen content and generally understood as a surrogate for SOA; BBOA: Biomass burning OA

Table 1. (cont). Summary of several literature studies of VBS treatments in various regional and global models.

Source	Bergstrom et al., 2012	Lane et al., 2008	Donahue et al., 2009	Murphy et al., 2009	This work
Model	EMEP	PMCAMx	PMCAMx	PMCAMx	WRF/Chem
Domain	Europe, a large part of the North Atlantic and Arctic areas	Eastern U.S.	Eastern U.S.	Eastern U.S.	CONUS with parts of Canada and Mexico
Spatial Resolution	50 km × 50 km	36 km × 36 km	NA	36 km × 36 km	36 km × 36 km
Emissions of SVOCs, IVOCs and VOCs	VOCs are present. S/IVOCs are 2.5 times the POA emissions	Only VOCs; SVOCs and IVOCs not added	Additional IVOCs added but details are not given	IVOC emissions are 0.2 to 0.8 times the nonvolatile POA emission rates	S/IVOCs are 1.5 to 3 times the nonvolatile POA NEI emissions
No. of VBS bins	4 for SOA components and 9 for POA	4	9	10	4 for SOA components and 9 for POA
Aging	Yes and No. Each oxidation step produces 7.5% additional mass	Yes. No additional mass produced for each oxidation step.	Yes. No additional mass produced for each oxidation step.	Yes. No additional mass produced for each oxidation step.	Yes. Each oxidation step produces 7.5% additional mass
Observational data	CARBOSOL, SORGA, Gote-2005	STN, IMPROVE	NA	STN, IMPROVE	STN, IMPROVE, field data
Variables evaluated	TC, OC	OA	POA, OPOA, SOA	OA	TC, OC, POA/OA
Summary of results with VBS framework with/without aging compared to the traditional SOA approach	-Addition of aging reactions improve summertime results but has little or negative consequences in wintertime -Deteriorations of model results with increased aging at urban influenced sites in southern Europe	-Addition of aging reactions overpredicts the OA concentrations in rural IMPROVE stations but improves the model performance in urban areas	-Aging results in better model predictions	-Slight overprediction with IMPROVE -Underprediction with STN	-Large improvements in predictions

Note: TC: total carbon; OC: Organic carbon; OPOA: oxidized POA

Table 2. Summary of main characteristics of CB05, CB6, and SAPRC07 gas-phase mechanisms.

	CB05-Cl[1]	**CB6**	**SAPRC07[2]**
No. of species	70	114	118
No. of reactions	156	218	599
Lumping method	Lumped structure based on carbon bonds	Lumped structure based on carbon bonds	Lumped species based on their reactivity towards hydroxyl (OH)
Kinetic Data for rate constants	Mostly from IUPAC (Atkinson et al., 2005). NASA/JPL (Sander et al., 2003) values were used in some cases where IUPAC data was not available.	New information from IUPAC (Atkinson et al., 2010) and NASA (Sander et al., 2006)	Mainly from IUPAC (2006) and NASA (Sander et al., 2006).
Photolysis data	Mainly from SAPRC99 chemical mechanism. IUPAC (Atkinson et al., 2005) was used if it differs significantly from SAPRC99.	New information from IUPAC (Atkinson et al., 2010) and NASA (Sander et al., 2006)	Mainly from IUPAC (2006) and NASA (Sander et al., 2006).
Ozone chemistry	Slightly underpredict O_3 mixing ratios with isoprene and in synthetic urban mixtures in chamber experiments.	Reduced underprediction in O_3 mixing ratios from benzene, toluene, and xylene, but forms O_3 from isoprene too slowly compared to CB05.	Slightly underpredict O_3 mixing ratios at low NO_x levels in chamber experiments.
Organic nitrate	2 reactions involving organic nitrate (NTR).	Additional NO_x recycling from organic nitrate to represent fate of NO_x over multiple days.	Added peroxy+NO reactions to form organic nitrate.
Chlorine chemistry	20 additional reactions for Cl chemistry involving species Cl_2, HOCl, Cl, ClO, and FMCl.	CB05 chlorine chemistry included in this work.	22 base chlorine reactions involving CL_2, CLNO, CLONO, $CLNO_2$, $CLONO_2$, HOCl, and 26 additional reactions involving organic products
Organic chemistry	- Explicit organic aerosol precursors, e.g., isoprene, toluene, xylene, α-pinene, ß-pinene.	- Explicit long-lived and abundant organic compounds including propane, acetone, benzene and acetylene added - Extensive revision of isoprene and aromatics chemistry -Formation of alpha-dicarbonyl compounds (glyoxal, glycoaldehyde, methylglyoxal) - Updates to peroxy radical chemistry that will improve formation of H_2O_2	- Reformulated reactions of peroxy radicals so that effects of changes in NO_x conditions on organic product formation is more accurately represented - Most comprehensive representation of VOCs compared to other gas-phase mechanisms
3-D host models	Implemented into WRF/Chem v3.6.1 by Wang et al. (2014). Also available in WRF/Chem v3.7.1	Implemented in CAMx by ENVIRON (2013)	Implemented in CMAQ (Carter, 2010)
Reference	Yarwood et al. (2005)	Yarwood et al. (2010) ENVIRON (2013)	Carter (2010)

[1] CB05 gas-phase mechanism with reactive chlorine chemistry (Yarwood et al., 2005)

[2] SAPRC07 uncondensed and expanded version C, which includes reactions for peroxy radical operators (Carter, 2010).

Table 3. Factors to calculate S/IVOC emissions from POA emissions from Shrivastava et al. (2011), May et al. (2013a, c) and newly calculated factors for this study.

Log Ci* at 298K	Normalized fraction for stationary emissions based on anthropogenic emissions from Shrivastava et al. (2011)	Fraction for gasoline emissions from May et al. (2013a)	Fraction for biomass burning emissions from May et al. (2013c)	New calculated fraction for all sources based on Shrivastava et al. (2011), May et al. (2013a, c), and % distribution of NEI emissions
-2	0.04	0.14	0.2	0.1754
-1	0.02	0.13	0.0	0.0141
0	0.03	0.15	0.1	0.0961
1	0.05	0.26	0.1	0.1084
2	0.07	0.15	0.2	0.1799
3	0.11	0.03	0.1	0.0949
4	0.16	0.02	0.3	0.258
5	0.20	0.01	0.0	0.0249
6	0.32	0.11	0.0	0.0483

Table 4. Configurations for OA and aerosol activation sensitivity simulations. All simulations except for CB05-SORG-DH contain the VBS treatments for OA.

Name	**Gas-Phase**	**ΔH_{vap}**	**VBS**	**FF**	**POA emissions**	**Aerosol activation**	**Cumulus Scheme**
CB05-SORG-DH	CB05	30 kJ mol^{-1}	-	-	Original NEI	ARG00	Grell-Freitas
CB05-VBS-DH	CB05	30 kJ mol^{-1}	SOA	-	Original NEI	ARG00	Grell-Freitas
CB05-POA-DH	CB05	30 kJ mol^{-1}	SOA/ POA	-	1.5×	ARG00	Grell-Freitas
CB05-POA	CB05	Epstein et al. (2010)	SOA/ POA	-	1.5×	ARG00	Grell-Freitas
CB05-50%FF	CB05	Epstein et al. (2010)	SOA/ POA	50%	1.5×	ARG00	Grell-Freitas
CB05-10%FF	CB05	Epstein et al. (2010)	SOA/ POA	10%	1.5×	ARG00	Grell-Freitas
CB05-25%FF	CB05	Epstein et al. (2010)	SOA/ POA	25%	1.5×	ARG00	Grell-Freitas
CB05-25%FF-EM3	CB05	Epstein et al. (2010)	SOA/ POA	25%	3.0×	ARG00	Grell-Freitas
CB6-25%FF-EM3	CB6	Epstein et al. (2010)	SOA/ POA	25%	3.0×	ARG00	Grell-Freitas
SAPRC07-25%FF-EM3	SAPRC07	Epstein et al. (2010)	SOA/ POA	25%	3.0×	ARG00	Grell-Freitas
CB05-25%FF-EM3 (FN05)	CB05	Epstein et al. (2010)	SOA/ POA	25%	3.0×	FN05	MSKF
CB05-25%FF-EM3 (FN05/ BA10)	CB05	Epstein et al. (2010)	SOA/ POA	25%	3.0×	FN05/ BA10	MSKF
CB05-25%FF-EM3 (MN14)	CB05	Epstein et al. (2010)	SOA/ POA	25%	3.0×	MN14	MSKF

The suffix "DH" in the case names refer to cases with the default ΔH_{vap} of 30 kJ mol^{-1}, otherwise with the semi-empirical correlation by Epstein et al. (2010). The simulations without the suffix "POA" or "FF" indicate cases with nonvolatile default POA emissions. The suffix "POA" in the case names refer to cases with semivolatile POA. The suffix "FF" in the case names refer to cases with semivolatile POA and with fragmentation and functionalization treatments, and the suffix "EM3" in the case names refer to cases with 3 times the original NEI POA emissions to take into account for missing S/IVOC species. "-" indicates not applicable.

Table 5. Range of statistics for OA/OC ratios of 1.4 and 2.1 (1.4/ 2.1) for May to June 2010. All simulations use the ARG00 aerosol activation scheme and the Grell-Freitas cumulus parameterization.

Case	Mean Obs	Mean Sim	Corr	NMB (%)	NME (%)
OC against IMPROVE					
CB05-SORG-DH	0.88	0.28/ 0.19	0.26	-68.1/ -78.7	73.9/ 80.9
CB05-VBS-DH	0.88	1.19/ 0.79	0.51	34.9/ -10.1	75.5/ 52.3
CB05-POA-DH	0.88	0.89/ 0.59	0.51	1.1/ -32.6	52.4/ 59.0
CB05-POA	0.88	1.05/ 0.70	0.51	18.9/ -20.7	63.2/ 49.2
CB05-10%FF	0.88	1.05/ 0.70	0.51	19.4/ -20.4	63.0/ 49.1
CB05-25%FF	0.88	0.86/ 0.57	0.49	-2.9/ -35.2	54.6/ 51.4
CB05-50%FF	0.88	0.56/ 0.37	0.45	-36.4/ -57.6	54.4/ 62.6
CB05-25%FF-EM3	0.88	1.09/ 0.73	0.47	23.8/ -17.5	65.9/ 50.2
CB6-25%FF-EM3	0.88	1.06/ 0.71	0.48	20.5/ -19.6	49.4/ 63.7
SAPRC07-25%FF-EM3	0.88	1.00/ 0.67	0.46	13.3/ -24.4	60.1/ 50.4
TC against IMPROVE					
CB05-SORG-DH	1.03	0.44/ 0.34	0.30	-57.6/ -66.7	67.9/ 72.3
CB05-VBS-DH	1.03	1.34/ 0.94	0.52	30.6/ -8.0	70.3/ 51.1
CB05-POA-DH	1.03	1.13/ 0.83	0.52	10.2/ -18.7	58.5/ 48.7
CB05-POA	1.03	1.29/ 0.94	0.53	25.6/ -8.5	63.8/ 48.3
CB05-10%FF	1.03	1.29/ 0.94	0.53	25.9/ -8.2	63.8/ 48.2
CB05-25%FF	1.03	1.09/ 0.83	0.51	6.8/ -21.6	55.2/ 48.2
CB05-50%FF	1.03	0.80/ 0.61	0.47	-22.0/ -40.2	50.8/ 53.4
CB05-25%FF-EM3	1.03	1.32/ 0.97	0.49	29.7/ -5.7	50.7/ 66.9
CB6-25%FF-EM3	1.03	1.30/ 0.95	0.50	27.2/ -7.3	65.2/ 50.0
SAPRC07-25%FF-EM3	1.03	1.23/ 0.90	0.48	20.6/ -11.9	61.4/ 49.4
TC against STN					
CB05-SORG-DH	2.71	1.34/ 1.10	0.29	-50.6/ -59.4	60.1/ 64.9
CB05-VBS-DH	2.71	3.35/ 2.44	0.47	23.7/ -5.8	53.1/ 42.0
CB05-POA-DH	2.71	2.88/ 2.19	0.47	6.2/ -19.0	45.5/ 41.6
CB05-POA	2.71	3.03/ 2.30	0.46	11.7/ -15.3	44.6/ 39.9
CB05-10%FF	2.71	3.03/ 2.30	0.46	11.8/ -15.3	44.5/ 39.8
CB05-25%-FF	2.71	2.66/ 2.05	0.44	-1.8/ -24.3	41.5/ 42.0
CB05-50%-FF	2.71	2.07/ 1.65	0.39	-23.8/ -39.1	43.9/ 49.4
CB05-25%FF-EM3	2.71	3.27/ 2.45	0.41	20.5/ -9.5	49.7/ 41.7
CB6-25%FF-EM3	2.71	3.39/ 2.45	0.34	24.9/ -6.4	54.8/ 45.5
SAPRC07-25%FF-EM3	2.71	3.00/ 2.28	0.41	10.7/ -16.1	45.2/ 42.0

Table 6. Statistics for evaluation at Bakersfield and Pasadena sites. A bar chart of daily average obs versus sim values can be found in Figure 4.

Case	Mean Obs	Mean Sim	Corr	NMB (%)	NME (%)
Bakersfield					
CB05-SORG-DH	0.51	5.9e-04	-0.15	-100	100%
CB05-VBS-DH	0.51	0.67	0.41	32.5	62.0
CB05-25%FF-EM3	0.51	0.24	-0.01	-52.0	61.0
CB6-25%FF-EM3	0.51	0.28	-0.04	-45.8	59.0
SAPRC07-25%FF-EM3	0.51	0.24	-0.16	-53.1	63.0
Pasadena					
CB05-SORG-DH	0.63	0.04	-0.07	-94.0	94.0
CB05-VBS-DH	0.63	0.54	0.09	-14.5	64.3
CB05-25%FF-EM3	0.63	0.54	-0.2	-14.4	66.2
CB6-25%FF-EM3	0.63	0.62	-0.2	-2.1	70.0
SAPRC07-25%FF-EM3	0.63	0.62	0.03	-1.4	70.5

Table 7. Statistics for max 1-h and max 8-h O_3 for simulations with different gas-phases against CASTNET and AQS for May to June 2010.

CASTNET Max 1-h O_3					
Case	**Mean Obs**	**Mean Sim**	**Corr**	**NMB (%)**	**NME (%)**
CB05-25%FF-EM3	51.8	43.3	0.54	-16.3	21.9
CB6-25%FF-EM3	51.8	41.9	0.52	-19.1	24.1
SAPRC07-25%FF-EM3	51.8	48.3	0.51	-6.7	21.1
CASTNET Max 8-h O_3					
Case	**Mean Obs**	**Mean Sim**	**Corr**	**NMB (%)**	**NME (%)**
CB05-25%FF-EM3	47.4	43.0	0.54	-9.3	18.9
CB6-25%FF-EM3	47.4	41.8	0.53	-11.8	20.6
SAPRC07-25%FF-EM3	47.4	47.9	0.50	1.0	19.8
AQS Max 1-h O_3					
Case	**Mean Obs**	**Mean Sim**	**Corr**	**NMB (%)**	**NME (%)**
CB05-25%FF-EM3	51.0	49.9	0.55	-2.1	18.2
CB6-25%FF-EM3	51.0	51.5	0.43	1.0	20.8
SAPRC07-25%FF-EM3	51.0	59.3	0.44	16.4	26.1
AQS Max 8-h O_3					
Case	**Mean Obs**	**Mean Sim**	**Corr**	**NMB (%)**	**NME (%)**
CB05-25%FF-EM3	46.2	46.0	0.54	-0.4	18.6
CB6-25%FF-EM3	46.2	47.4	0.47	2.6	20.3
SAPRC07-25%FF-EM3	46.2	53.7	0.46	16.3	25.4
IMPROVE $PM_{2.5}$					
Case	**Mean Obs**	**Mean Sim**	**Corr**	**NMB (%)**	**NME (%)**
CB05-25%FF-EM3	4.9	3.8	0.64	-22.0	40.6
CB6-25%FF-EM3	4.9	4.1	0.65	-16.5	39.6
SAPRC07-25%FF-EM3	4.9	3.5	0.60	-28.5	42.9
STN $PM_{2.5}$					
Case	**Mean Obs**	**Mean Sim**	**Corr**	**NMB (%)**	**NME (%)**
CB05-25%FF-EM3	11.1	8.8	0.48	-20.6	40.7
CB6-25%FF-EM3	11.1	10.0	0.37	-9.3	44.3
SAPRC07-25%FF-EM3	11.1	7.7	0.40	-30.5	45.2
AQS PM_{10}					
Case	**Mean Obs**	**Mean Sim**	**Corr**	**NMB (%)**	**NME (%)**
CB05-25%FF-EM3	24.6	7.3	0.08	-70.2	73.5
CB6-25%FF-EM3	24.6	8.0	0.09	-67.7	71.8
SAPRC07-25%FF-EM3	24.6	6.9	0.09	-71.9	74.8

Table 8. Statistics for model evaluation for simulated CDNC against MODIS-derived CDNC from Bennartz (2007). All cases use the Grell-Freitas cumulus parameterization.

Case	Mean Obs	Mean Sim	Corr	NMB (%)	NME (%)
CB05-SORG-DH	162.1	96.0	0.28	-40.8	50.4
CB05-VBS-DH	162.1	106.0	0.28	-34.6	50.6
CB05-POA-DH	162.1	115.0	0.29	-29.1	47.4
CB05-POA	162.1	117.3	0.29	-27.7	47.3
CB05-10%FF	162.1	117.1	0.29	-27.8	47.2
CB05-25%-FF	162.1	116.4	0.29	-28.2	47.3
CB05-50%-FF	162.1	114.7	0.29	-29.2	47.4
CB05-25%FF-EM3	162.1	116.2	0.29	-28.3	47.3
CB6-25%FF-EM3	162.1	110.4	0.30	-31.9	47.3
SAPRC07-25%FF-EM3	162.1	77.3	0.26	-52.3	55.8

Table 9. Statistics for simulated CDNC for CB05-25%FF-EM3 against MODIS-derived CDNC from Bennartz (2007) for May to June 2010. All cases use the MSKF cumulus parameterization.

Case	Mean Obs	Mean Sim	Corr	NMB (%)	NME (%)
ARG00	162.1	104.8	0.31	-35.4	49.9
FN05	162.1	173.8	0.26	7.1	93.0
FN05/BA10	162.1	160.8	0.27	-0.8	87.9
MN14	162.1	168.9	0.27	4.2	89.6

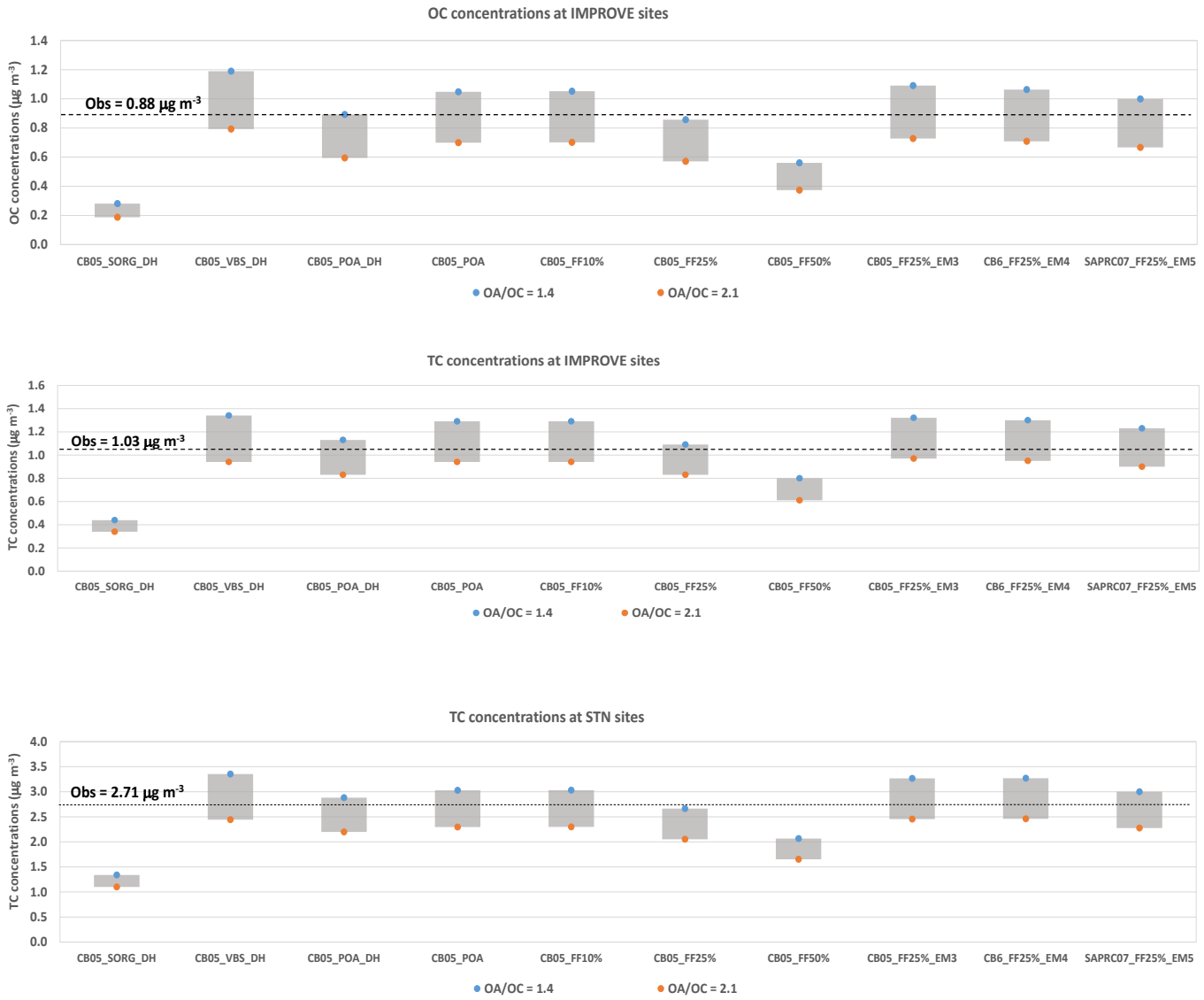

Figure 1. Sim OC and TC concentrations against observations from IMPROVE and STN under two OA/OC ratios: 1.4 and 2.1, , resulting in a range of possible OC or TC values denoted by the gray bars. The obs OC or TC is denoted by the horizontal dotted line.

IMPROVE OC (markers) with Sim OC (background) with OA/OC = 2.1

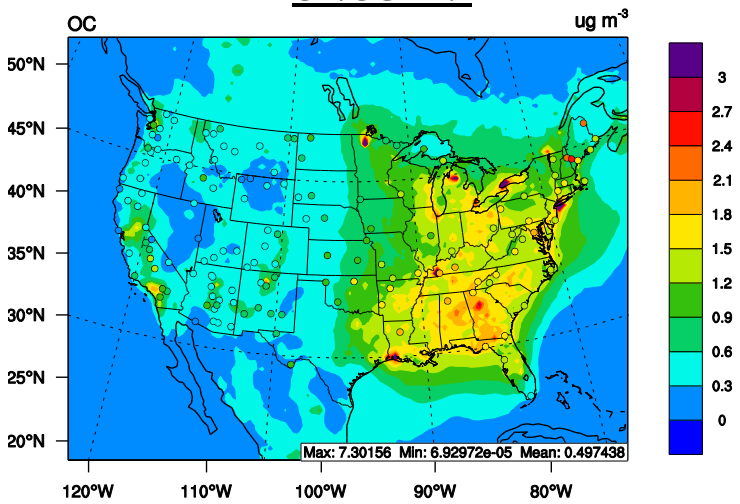

STN TC (markers) with Sim TC (background) with OA/OC = 2.1

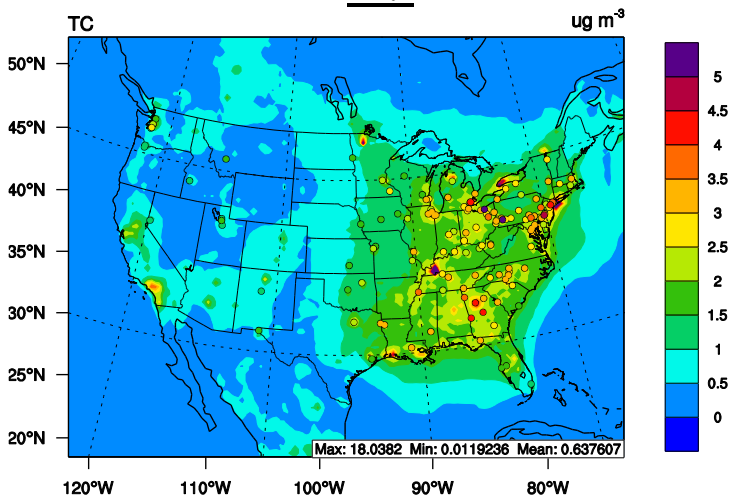

IMPROVE OC (markers) with Sim OC (background) with OA/OC = 1.4

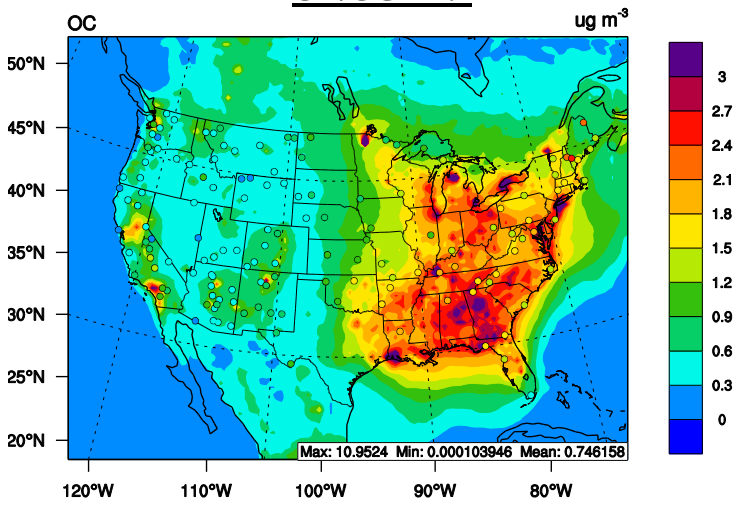

STN TC (markers) with Sim TC (background) with OA/OC = 1.4

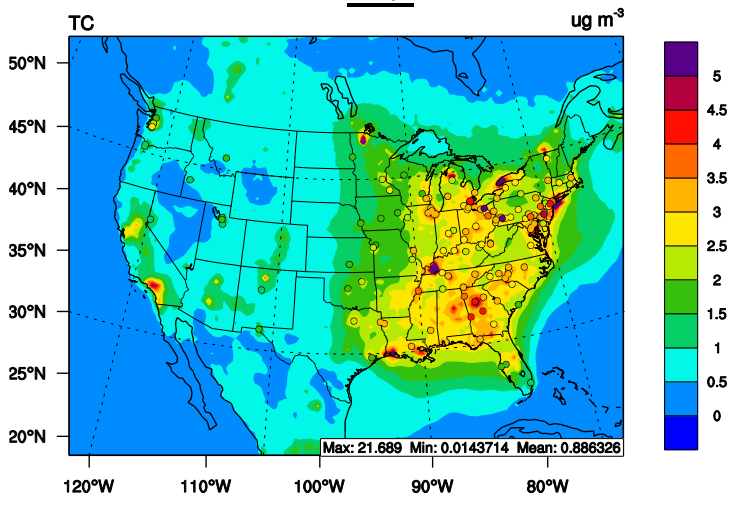

Figure 2. Overlay of obs data (markers) versus sim data (background) for IMPROVE OC and STN TC and for OA/OC ratios of 1.4 and 2.1 for the case CB05_25%FF_EM3.

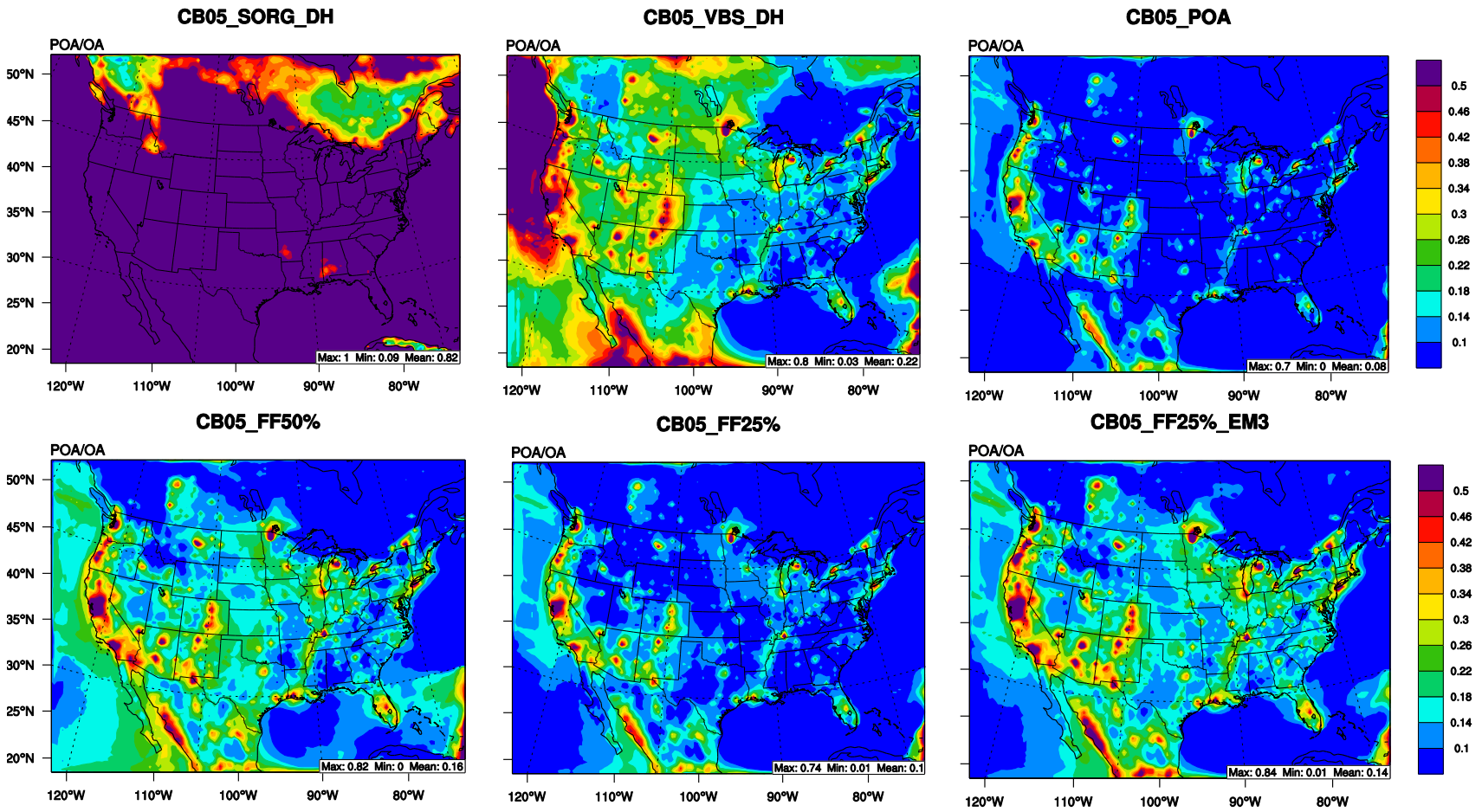

Figure 3. POA/OA ratios of sim data from various sensitivity simulation cases.

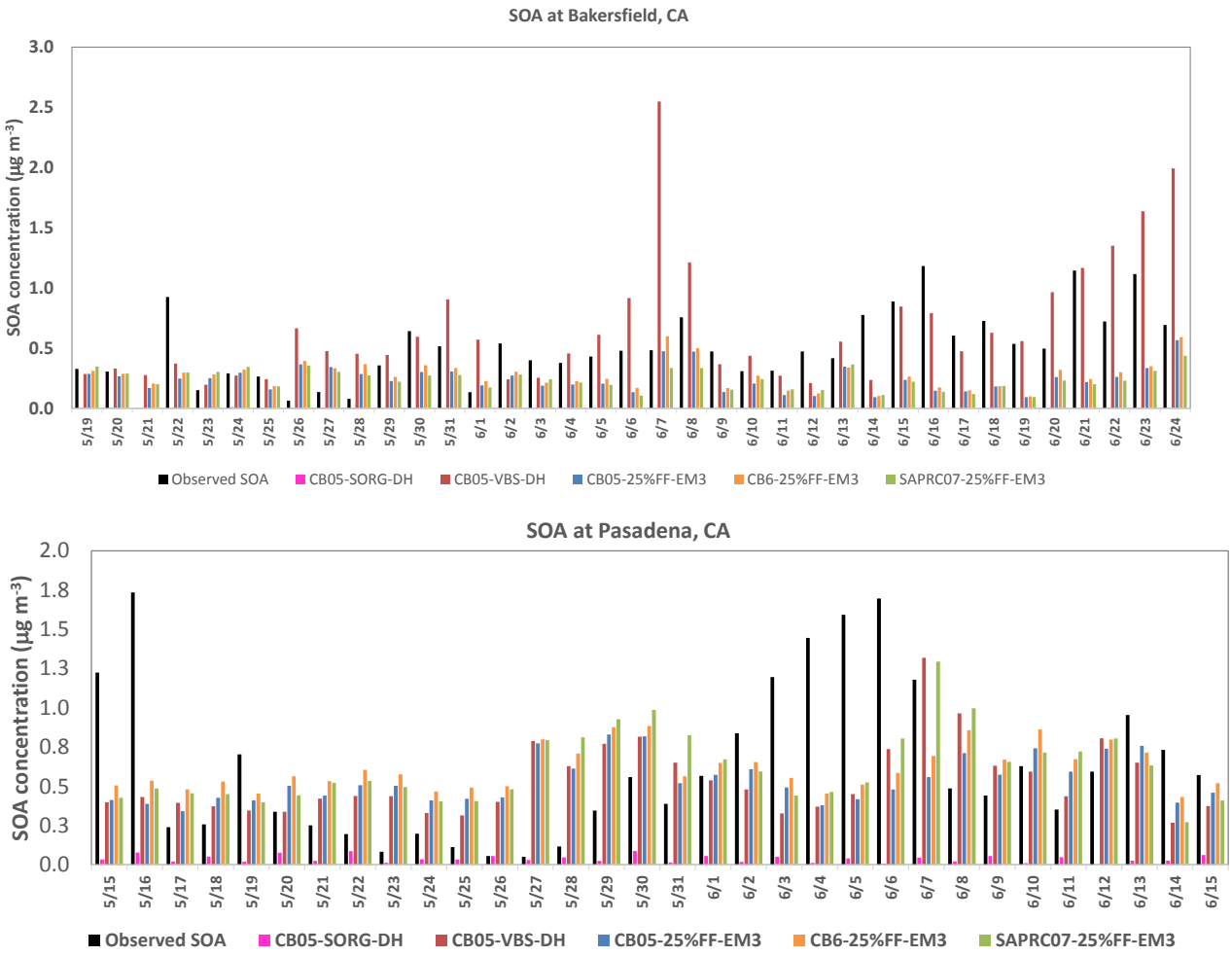

Figure 4. Comparison of obs SOA versus sim SOA at CalNex sites in Bakersfield and Pasadena in California.

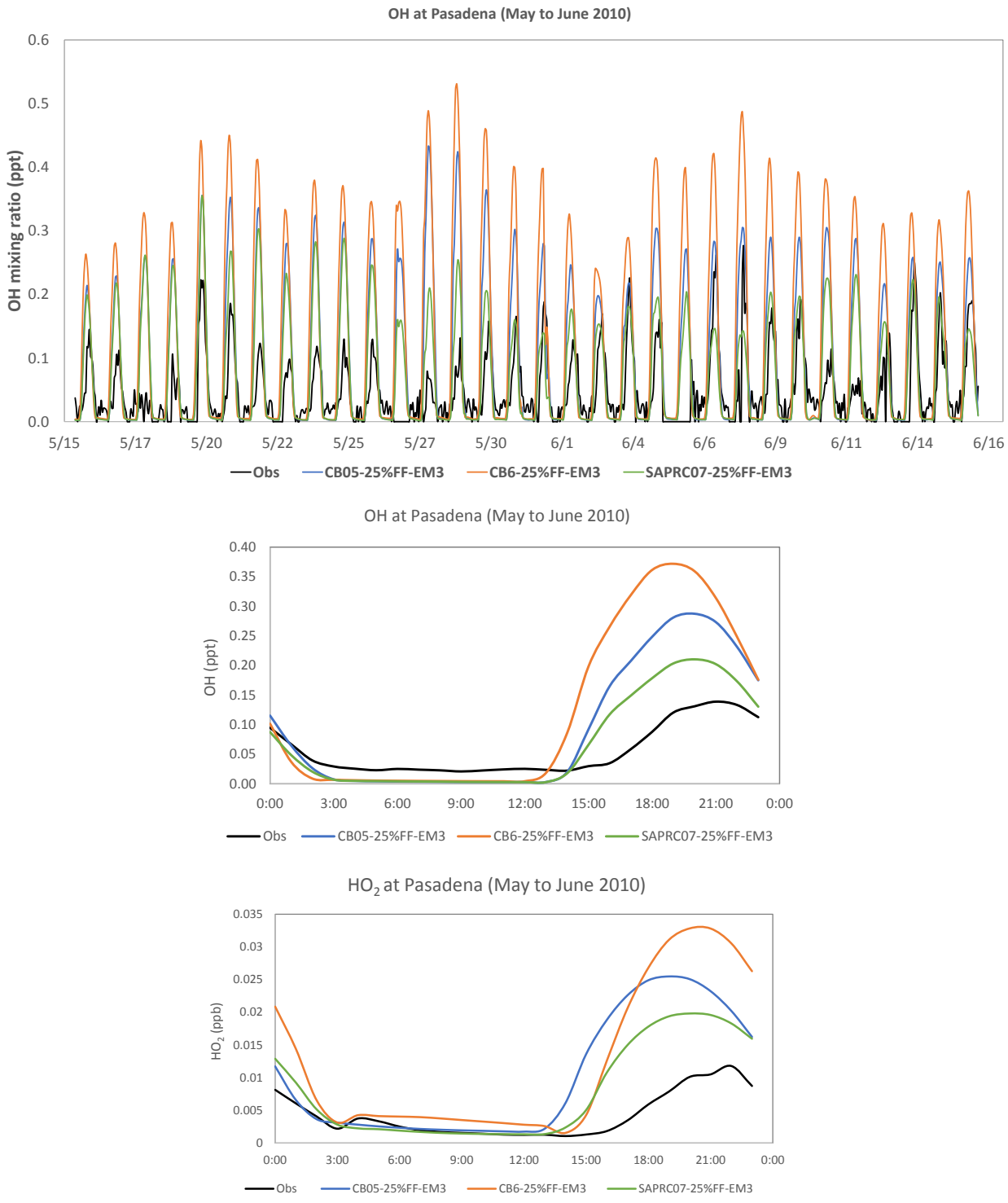

Figure 5. Time series of OH and diurnal plots of OH and HO_2 at Pasadena, CA during CALNEX, 2010.

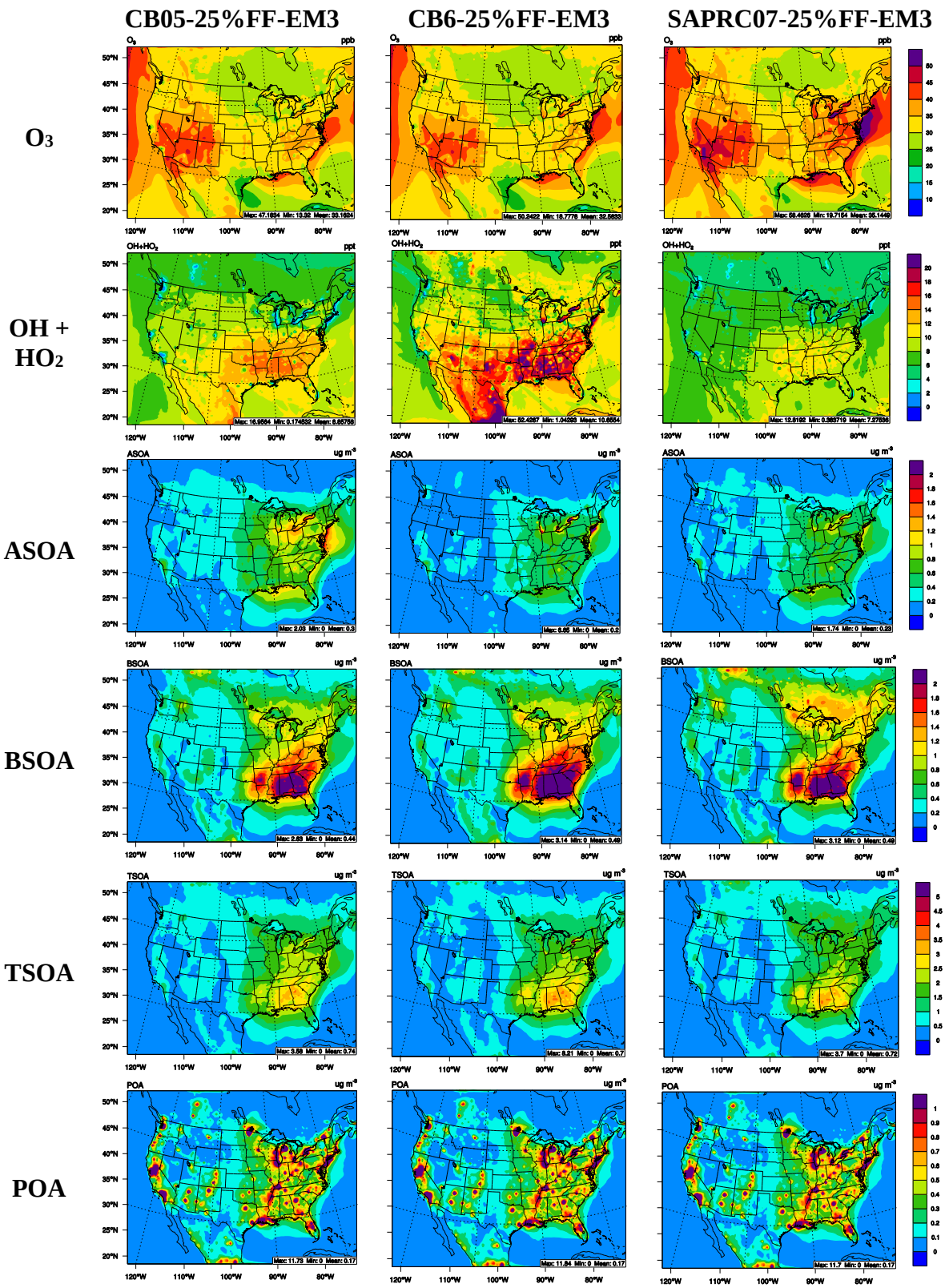

Figure 6. Spatial plots of several gas and aerosol species for the three cases with different gas-phase mechanisms.

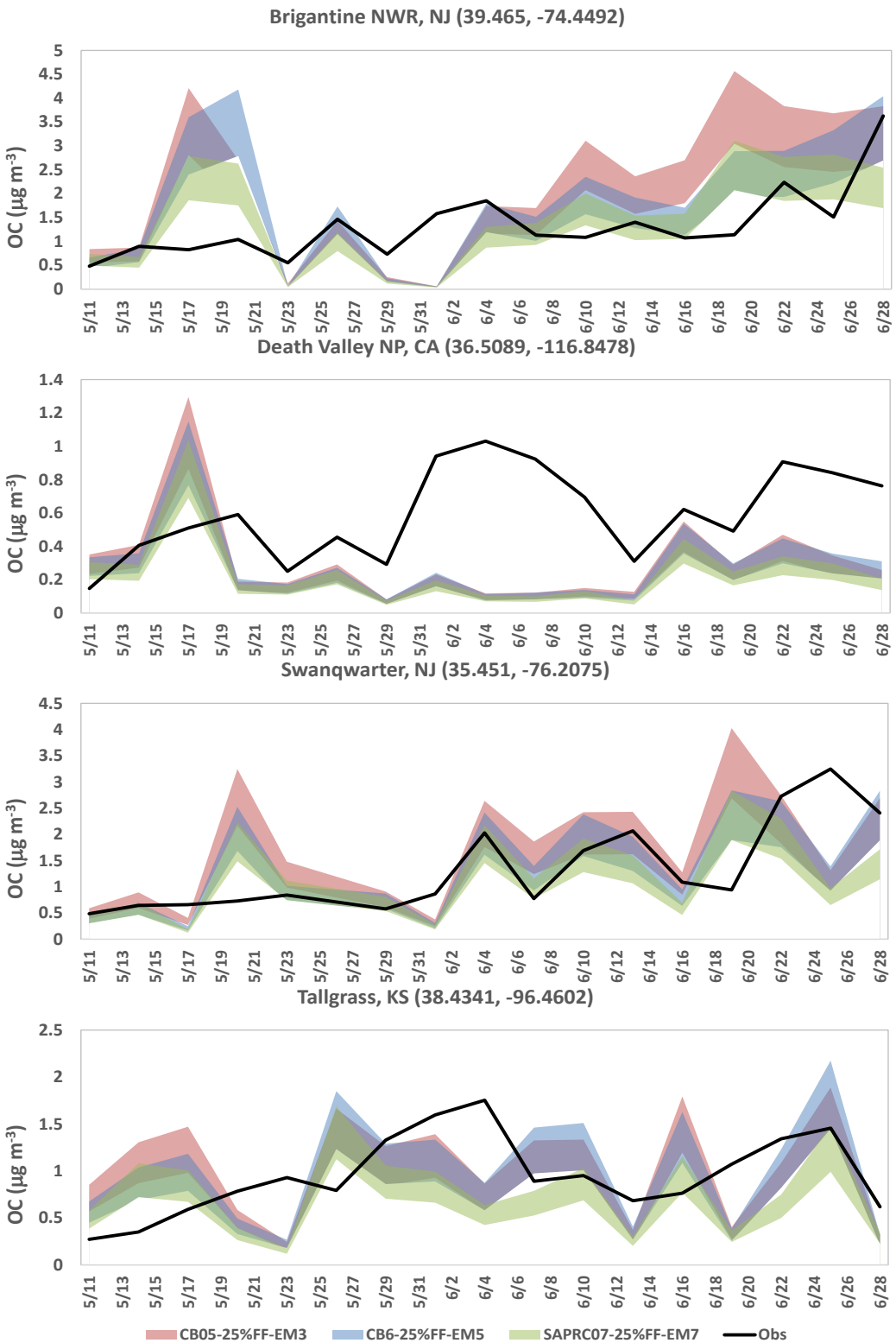

Figure 7. Timeseries plots of IMPROVE OC versus simulated OC at selected sites from sensitivity simulations of different gas-phase mechanisms. The colored bands represent the range of OC values for ratios 1.4 to 2.1.

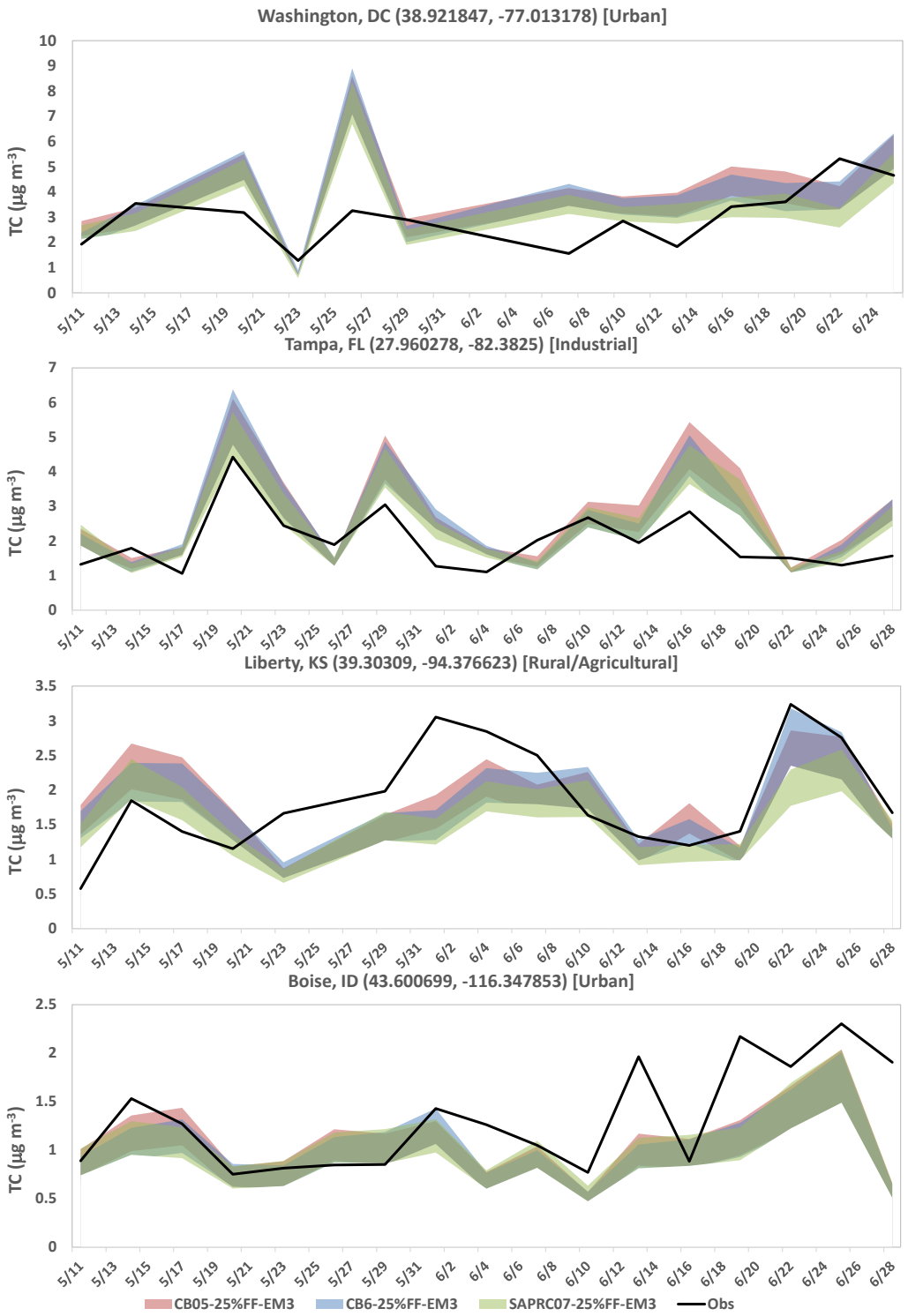

Figure 8. Timeseries plots of STN TC versus simulated TC at selected sites from sensitivity simulations of different gas-phase mechanisms. The colored bands represent the range of OC values for ratios 1.4 to 2.1.

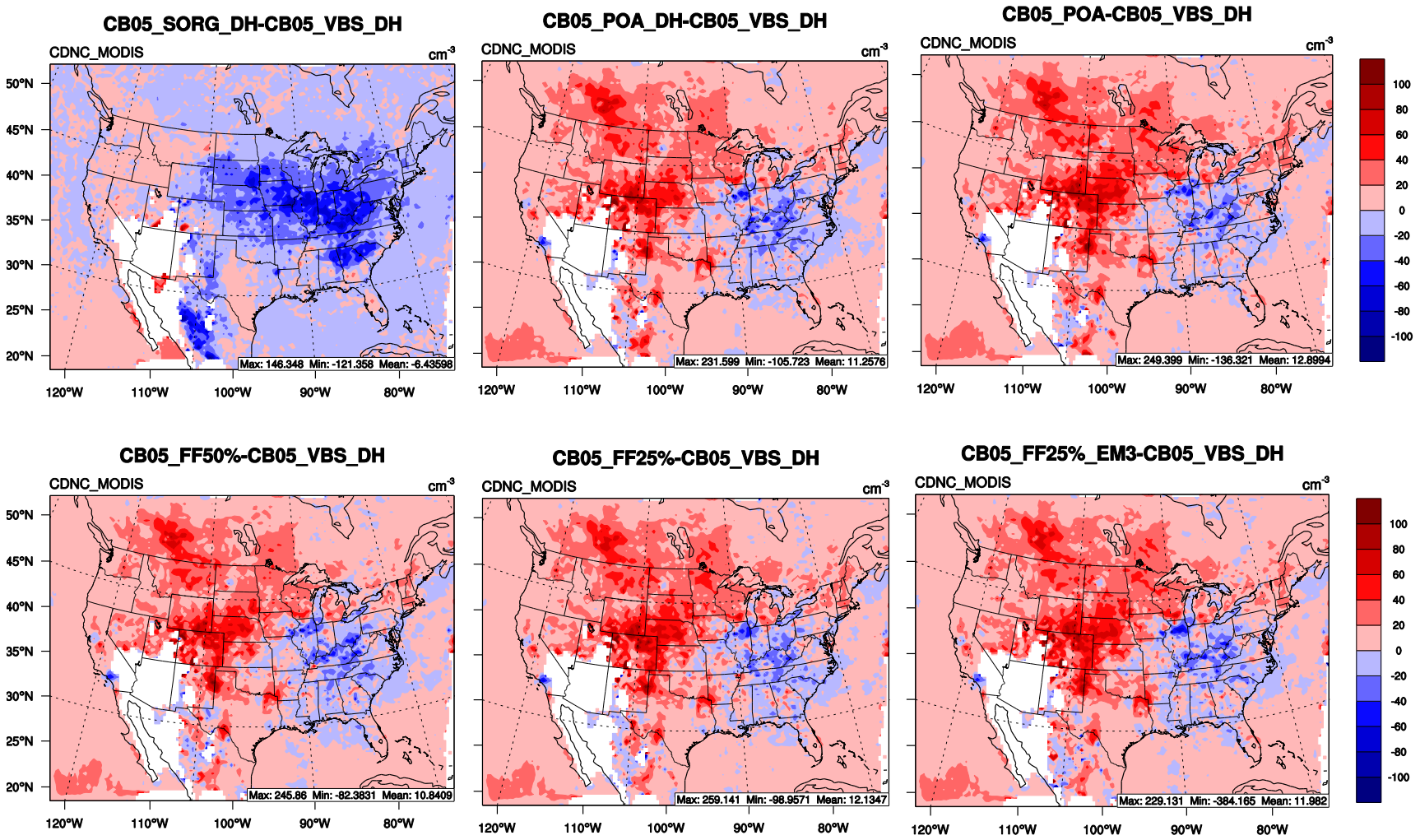

Figure 9. Impact of different VBS case on CDNC in warm clouds. The plots show the differences between the different sensitivity simulations and CB05_VBS-DH.

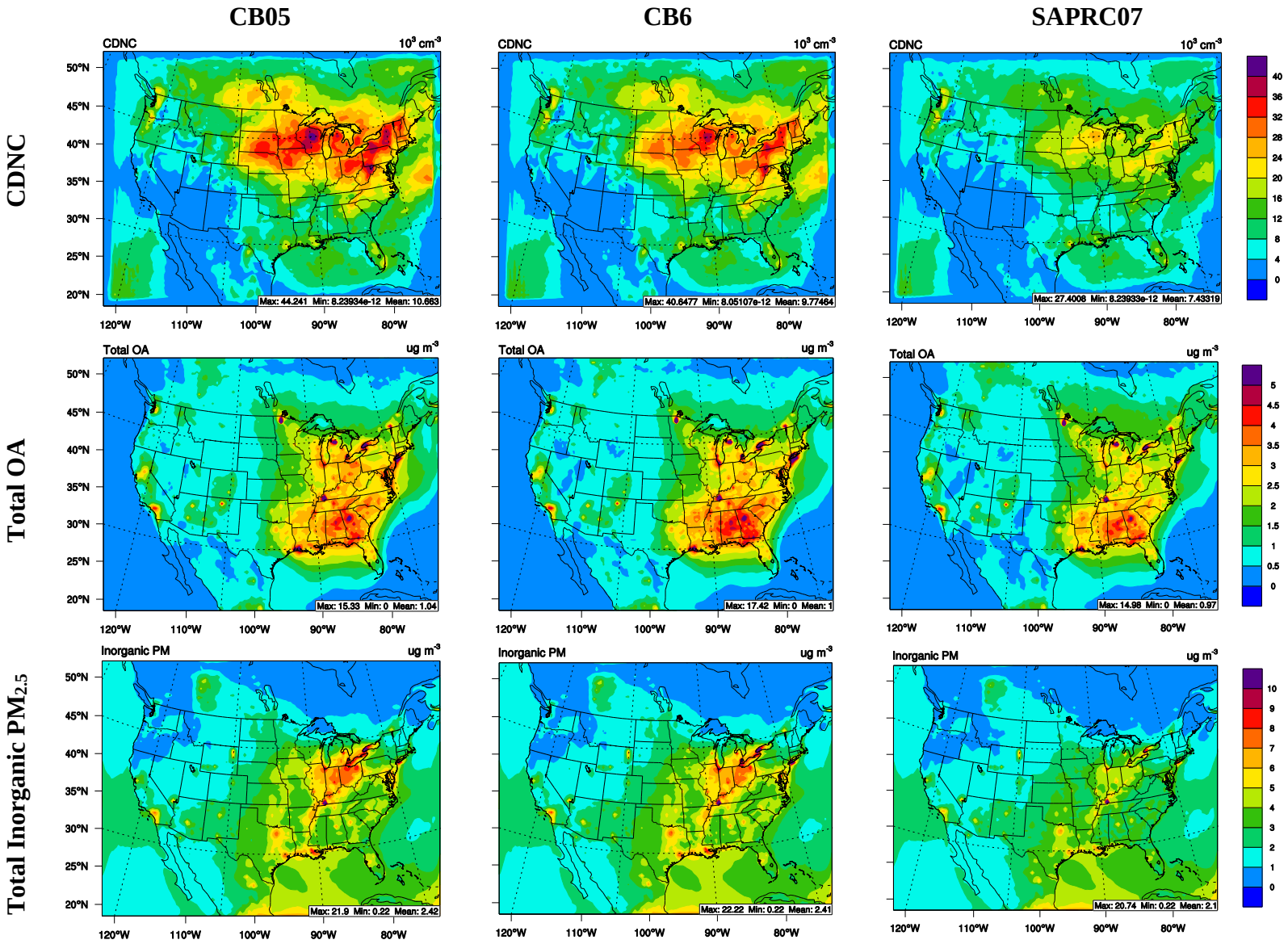

Figure 10. Spatial plots of CDNC, total surface OA and total inorganic $PM_{2.5}$ concentrations from different gas-phase mechanisms.

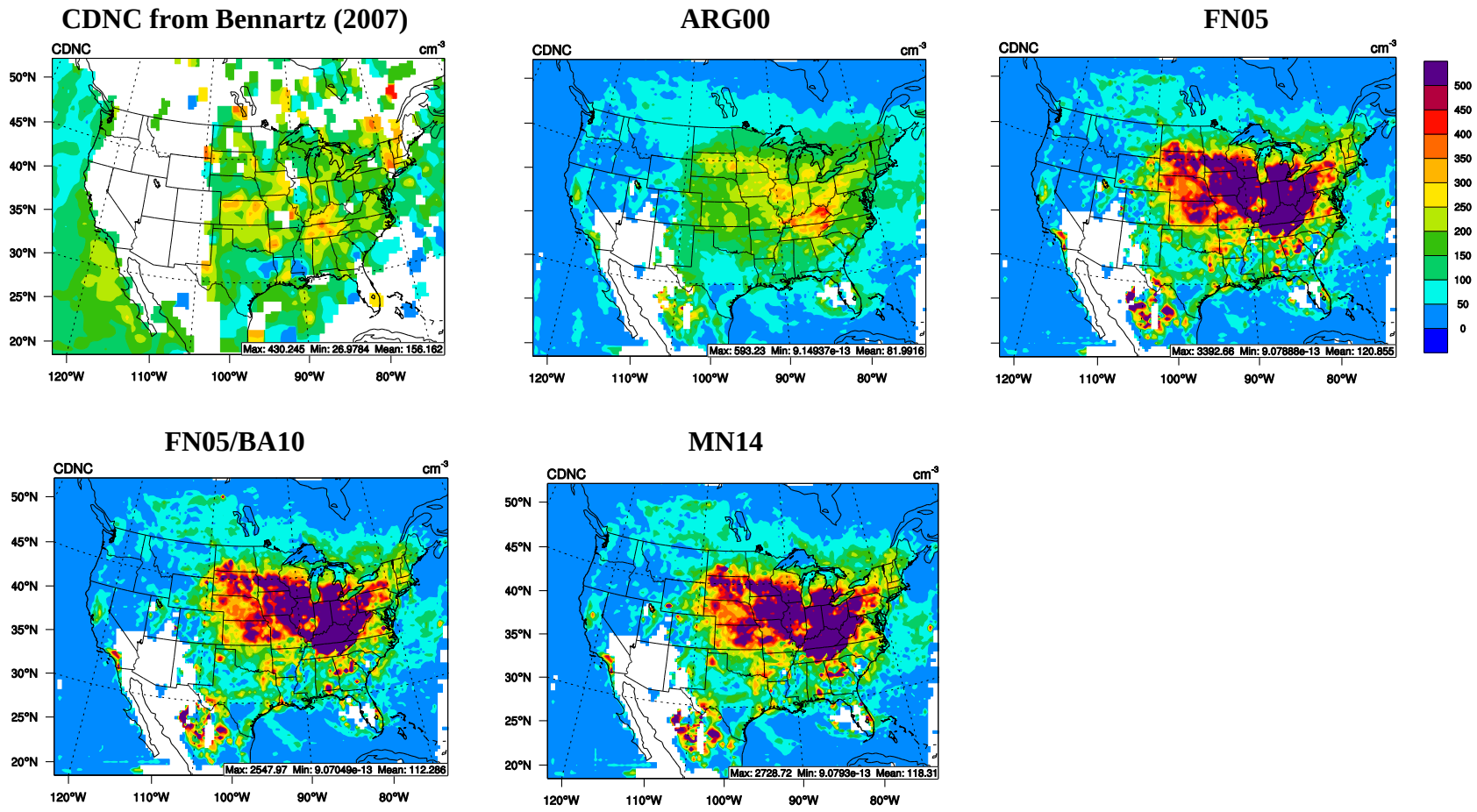

Figure 11. Spatial plots for MODIS-derived CDNC from Bennartz (2007) and simulated CDNC from CB05_25%FF_EM3 ARG00, FN series, and MN14 from May to June 2010.

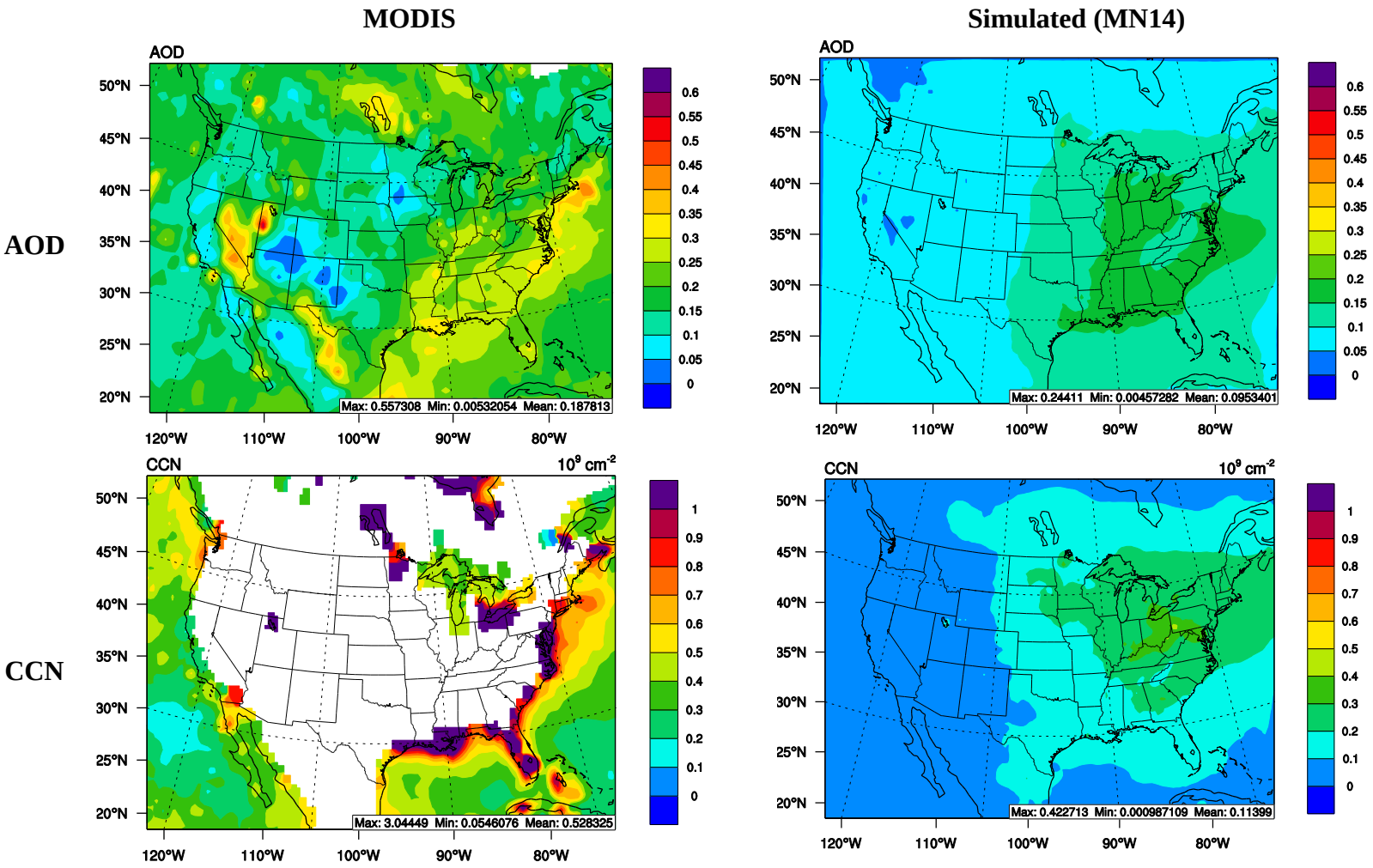

Figure 12. Plots of MODIS AOD and CCN against simulated AOD and CCN from MN14 with CB05_25%FF_EM3.